REGENERATIVE PERIPHERAL NEUROINTERFACING OF UPPER EXTREMITY PROSTHESES

by

KSHITIJA GARDE

Presented to the Faculty of the Graduate School of

The University of Texas at Arlington in Partial Fulfillment

of the Requirements

for the Degree of

MASTER OF SCIENCE IN BIOMEDICAL ENGINEERING

THE UNIVERSITY OF TEXAS AT ARLINGTON

August 2008

ACKNOWLEDGEMENTS

I would like to thank my family for the opportunity to pursue higher education in United States and who always trusted my decisions. I would gladly take this opportunity to express my gratitude to my mentor Dr. Mario Romero-Ortega who gave me the opportunity to work and introduced me to the field of Neurobiology. He always helped and guided me throughout my work and encouraged me to give my best in all aspects. He has enabled my transition from being a proletarian to be a professional in the field of scientific research. His guidance was very precious to me and helped me developing scientific maturity in the field of Neurobiology.

I would also like to thank Dr. Edward Keefer who introduced me to the practical/ industrial research where I learned how basic scientific principles are applied to solve real-life problems. As my co-mentor he taught me how to think logically and to derive scientific conclusions from the observations. His advice helped me to solve tough practical problems and take important decisions. He has also taught me how to efficiently integrate engineering and biology. I would also like to express sincere gratitude to Harvey Wiggins who introduced me to the industrial ambience and gave me an opportunity to seek research experience at Plexon Inc.

I am always thankful to all my colleagues from Texas Scottish Rite Hospital and the Plastic Surgery department, UTSW especially Cheng-yu Ko who helped me like a friend. I am also thankful to Dr. Barry Botterman who offered his lab space and guidance

in the electrophysiology studies. I would like to thank Myresa Hurst, animal surgeon and Reuel Cornelia, senior histologist for their technical expertise. I am grateful to Russ Daniel, lab manager for providing all the necessary resources required for my experiments. Finally, I would like to thank all my friends to have supported me morally through my thick and thins.

July 1, 2008

ABSTRACT

REGENERATIVE PERIPHERAL NEUROINTERFAING OF UPPER EXTREMITY PROSTHESES

Kshitija Garde, M.S.

The University of Texas at Arlington, 2008

Supervising Professor: Mario Romero-Ortega, PhD

Current robotic prosthetic devices provide limited functionality to the user as they rely on gross myogenic control and lack critical sensory feedback needed for fine movement control. Interfacing the nervous system with the robotic prosthesis would facilitate amputees to control them naturally, in resemblance to the human hand. Functional neuro-electrode connections have been demonstrated in the brain and peripheral nervous system; however, gliosis, micro hemorrhages, axonopathy and excessive inflammation limit their long-term use. We evaluated the possibility of enticing peripheral nerve regeneration through a multi-electrode array with an open architecture as an alternative to enhance longevity of nerve-electrode interface. Regenerative conduits

deploying 18-electrode arrays were implanted into the transected sciatic nerve of acute and chronic (n=6) injured adult rats, and electrophysiological recordings, behavioral and histological analysis were performed at 19-223 days post implantation. In both acute and chronic implanted animals, axons regenerated in close proximity (10-150 μm) to the electrodes. Myelinated and ummyelinated axons were visualized by double-immunostaining of myelin basic protein and calcitonin gene related peptide; respectively. The accumulation of activated macrophages (ED1+) was limited to 2-3 cell layers coating the electrodes. Behavioral studies showed partial motor function recovery in acute injury group, demonstrating the ability of the interfaced peripheral nerves to reconnect with their original target organs. Action potentials in a form of single/multi-unit activity from regenerating axons were recorded as early as one week, and up to two months post implantation, with high signal to noise ratio (SNR).

We also sought to segregate different sub-types of regenerating axons via specific growth factors induction. Successful enrichment of pain and proprioceptive sensory fibers was achieved by nerve growth factor and NT-3 stimulation respectively. Finally we worked in improving the electrode array itself, as those used are made of conductive metal. In order to enhance the electrochemical stability of these implantable electrodes, we used conductive nanomaterials to augment the sensitivity of the implant. Together, our findings support the notion that regenerative multi-electrodes would provide an enhanced neurointerface for the control of robotic prosthesis.

TABLE OF CONTENTS

LIST OF ILLUSTRATIONS

LIST OF TABLES

CHAPTER 1

INTRODUCTION

1.1 Significance

There are over 1.7 million amputees in United States with approximately 185,000 of annual increment in the amputee patients (Ziegler-Graham 2005) out of which 10% comprises of upper extremity amputees. It has been reported that United States alone has 10,000 new upper extremity amputees every year due to war-related or accident-related injuries. Amputation rates due to combat related injuries in soldiers were constant through American Civil war, Korean War and World War but have drastically increased recently in Vietnam and Iraq wars (Potter 2006). Upper limb amputees are the most affected ones due to their loss of ability to perform simple daily chores. In addition to biopsychological and pharmacological treatments, recent advancements in prosthetic devices would assist these patients to lead a normal life by replacing their missing limb with functional prostheses.

There are different types of upper limb amputations each having its own set of desired performance requirements for the prostheses. The level of amputations varies from transphalangeal (finger resection), transradial (below elbow), transhumeral (above elbow), elbow disarticulation (at elbow joint) to shoulder disarticulation (at shoulder joint). The ideal prosthesis has to be modular facilitating easy customization for any level

of amputation, lightweight to reduce inconvenience, agile to provide dexterity of the hand and controllable so that patients feel it as their natural hand/arm.

The human hand has a complex anatomical and physiological structure with extensive range of functions and 21 degrees of freedom. These functions can be grouped into non prehensile (touching, feeling, tapping) and prehensile activities (three-jaw, and lateral or key grip, power grip, hook grip and spherical grip). Development of upper extremity prosthesis is much complex than lower limb prosthesis due to its functional complexity. Several upper limb prostheses have been developed such as artificial hands, wrists, arm and hooks (Fig 1.1A); however these devices did not have volitional control. Body powered prostheses were subsequently developed where a harness-based control provided limited degree of movements (Fig 1.1B). More recently, myoelectric prostheses were developed (Fig 1.1C) to provide increase functionality. Such prosthetic devices consists of motorized hands, hooks or wrists which are controlled by acquiring electric signals generated by contracting muscles of the residual limb. It works well for transradial amputees but cannot be used in amputees with shoulder disarticulation.

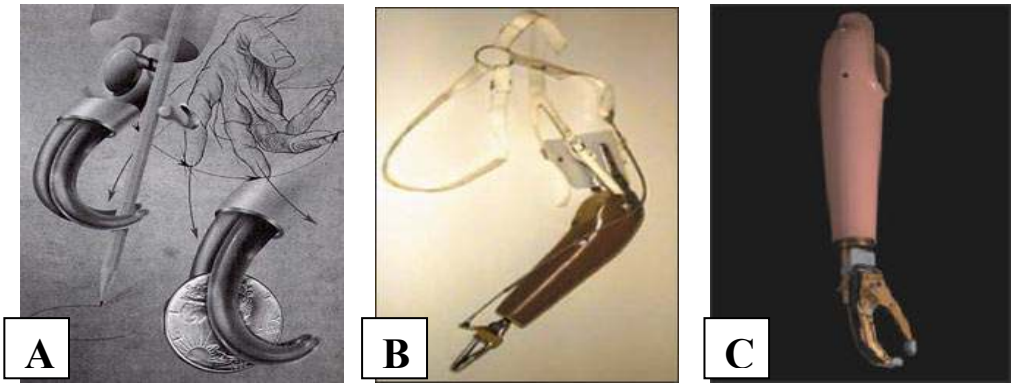

Figure 1.1 Development of upper extremity prostheses: A shows a passive hook based terminal device used in early 20th century. B shows mechanically (harness) controlled upper extremity prostheses C shows an example myoelectrically powered prosthesis.

Absence of proprioceptive feedback (information about limb location in the space) requires the patient to control motion of the prosthesis by vision, which resulted in poor coordination, declining accuracy of the prosthesis and exhausted the patient. Also myoelectric prosthesis has the ability to perform only one function at a time.

Current efforts are directed towards improving the degrees of freedom and incorporate complete functionality to the upper arm prosthetics. Connecting robotic prosthetic devices to the nervous system has been proposed as a better mechanism to enable patients to naturally control its motor output by sensory feedback control and feel bionic limbs in close resemblance to the human arm/hand.

1.2 Various approaches to develop neuroprostheses

1.2.1 Target Muscle Reinnervation

Dr. Todd Kuiken at the Rehabilitation Institute of Chicago developed the Targeted Muscle Reinnervation (TMR) technique by which the amputated nerves are grafted on-to pectoral muscles proximal to stump (Kuiken 2003). Electromyogenic signals acquired from the contracting re-innervated muscle are then used to control robotic prosthesis. Using the TMR technique several subjects have shown functional improvements like faster speed and simultaneous control compared to conventional prostheses (Miller et al. 2008). Despite the fact that referred perceptions can be elicited by electrical and mechanical stimulation of the chest muscles (Kuiken et al. 2007), these can be cumbersome and inefficient as large current/voltages are required.

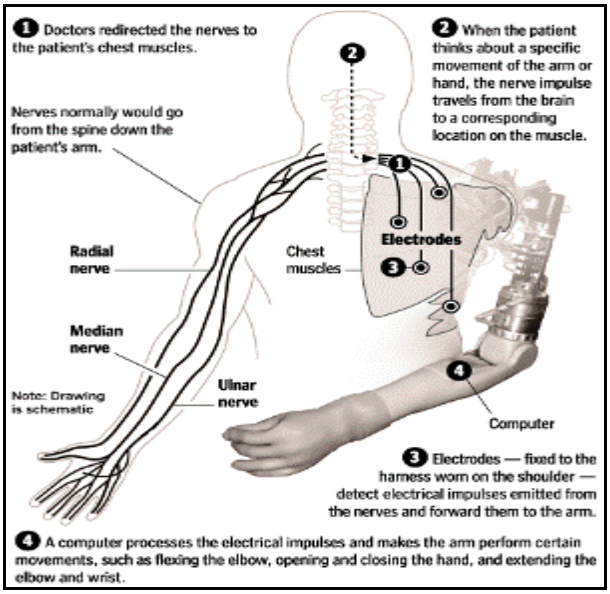

Figure 1.2 Schematic of Target Muscle Reinnervation: Median and radial nerves are redirected to grow in remaining muscle from where electromyographic signals are obtained and processed to perform certain actions in response to their thought.

1.2.2 Brain-machine interface

Electrical coupling with the brain to decode its activity as it relates to planned motor signals, can be used to control the movement of robotic prosthetic devices (Schwartz 2004). This so called, brain-machine interfaces were first conceived more than 30 years ago, when Evarts demonstrated the possibility to record from cerebral neurons and correlate the changes in firing pattern with EMG signals collected during specific movements (Evarts 1966). Further advancements lead to the development of cortical neural prostheses (CNPs), which use chronic recording microelectrode arrays to record from multiple neurons (Donoghue 2002; Lauer et al. 2000; Nicolelis 2001; Schwartz 2004), and used to decipher the voluntary movements and control the prosthetic devices (Donoghue et al. 2007; Lebedev and Nicolelis 2006; Mussa-Ivaldi and Miller 2003;

Nicolelis 2003; Normann 2007; Patil and Turner 2008). This technology has been shown to enable a paraplegic patient to move a computer cursor by thought (Hochberg et al. 2006). However, signals recorded from the cortical neurons deteriorate over time due to adverse tissue reactions compromising the long-term use of BMI (Biran et al. 2007; Griffith and Humphrey 2006; Szarowski et al. 2003). Furthermore, providing sensory feedback via BMI is challenging since electrical stimulation on the transected nerve results in mixed somatosensory representations (Nicolelis et al. 1995). Such limitations lead to the development of peripheral nerve interfacing.

1.2.3 Peripheral Neuroprostheses

A selective neurointerface for the control of artificial limbs requires the ability of recording command information from motor neurons and safely stimulating sensory axons to convey needed information for precise motor control and other sensory modalities (i.e. pain, light touch, mechanoception). This can be achieved by electrically interfacing peripheral nerves (Loeb and Peck 1996; Rutten 2002; Slot et al. 1997). Peripheral interfaces can provide recordings from motor fibers and also the opportunity to selectively stimulate sensory afferents to convey haptic and sensory information from the robotic prosthesis. Human volunteer studies have demonstrated that direct electrical stimulation of single afferent units from the median nerve above the elbow gives rise to a clear sensation of mechanical deformation of skin, vibrations (Torebjork 1985; Vallbo et al. 1984) and pain (Torebjork 1985). Similar studies were done in which sensory fascicle of the median nerve from the residual limb was stimulated which produced sensation in

the thumb (Riso 1999). Thus, the use of peripheral microelectrode arrays is a reasonable alternative to develop bi-directional neurointerfaces.

1.2.4 Organization of the peripheral nervous system

Nerves from the brain and the spinal cord form the peripheral nervous system (PNS). Nerve fibers bundle within the endoneurium and are wrapped in a perineurium layer of fibroblasts and collagen forming fascicles, in turn surrounding by an epineurium fibrocollagenous tissue to form nerve trunk (Schmidt and Leach 2003). The perineurium acts as a diffusion barrier due to presence of tight junctions which aid in maintaining microenvironment of endoneurial space.

There are myelinated and non-myelinated neurons associated with Schwann cells, glial cells found in the PNS. In myelinated neurons, areas of Schwann contact form the nodes of Ranvier where exchange of extracellular ions takes place. This kind of signal transmission from nodes to nodes and within insulated myelin sheath underlies the saltatory propagation of action potentials. In the PNS, fibers are also classified based on their fiber diameter and conduction velocity (CV). Fibers are divided into Aα efferent motor (12-20 um), Aβ proprioceptive (2-5 um), Aγ touch and pressure, (3-6 um), Aδ motor fibers innervating muscle spindles, and C fibers for noxious heat and pricking pain perception (Lundborg 2004).

1.2.5 Cuff electrodes

Compound action potentials can be recorded from silicon or polyimide cuff electrodes; these are tubes with luminal recording sites that cover the nerve (Fig 1.4A-B). Compared to other invasive intraneural electrodes, cuff electrodes are relatively easy to

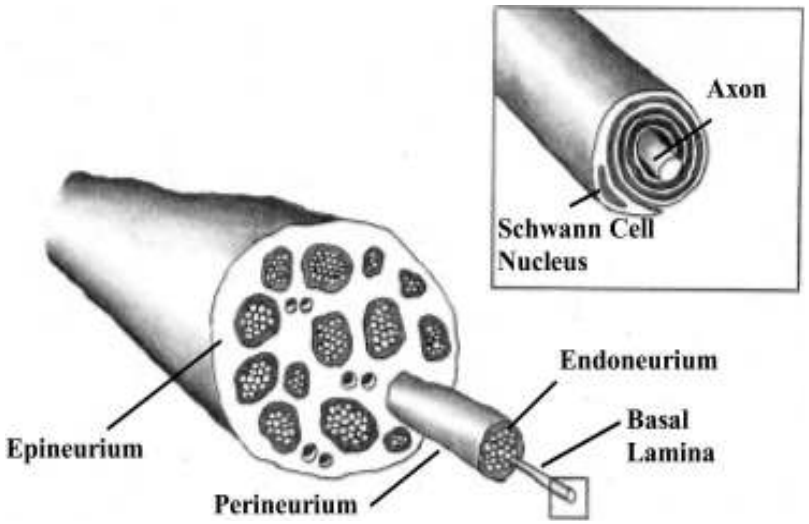

Figure 1.3: Schematic representation of a peripheral nerve organization: Peripheral nerve consists of axons which are surrounded by Schwann cells. These bundled up to form fascicles which are covered by perineurium. Outermost layer consists of epineurium and fibroblasts. Figure adapted from Schmidt and Leach, 2003.

implant with less probability for nerve damage (Loeb and Peck 1996; Navarro et al. 2001; Slot et al. 1997).

Efficient charge injection with specificity was difficult to achieve in this type of interface. The accessibility of the electrodes to the nerve fascicles was increased by flattening the nerve in the flat interface nerve electrode (FINE, 1.4C) interface developed by Durand and his colleagues to facilitate selective stimulation of the fibers (Tyler and Durand 2003; 2002). Stable long-term recordings from these electrodes is affected by the excessive connective tissue growth and epineurial fibrosis that form and which limits the efficiency of the cuff electrodes to record and stimulate (Vince et al. 2005).

1.2.6 Intrafascicular Penetrating electrode

Intrafascicular electrodes were developed to achieve better topographical selectivity, high-density and high-spatial resolution sampling of neuronal activity as compared to extraneural electrodes. Longitudinally implanted intrafascicular electrodes (LIFE) made of 25μm Pt/Ir insulated wires, were used to interface peripheral nerves to the external machines. This system provided appropriate, graded, distally referred sensations of touch and joint movement and natural motor control mechanism in experimental as well as clinical studies (Dhillon and Horch 2005; Dhillon et al. 2005; Li et al. 2005). With the idea of multi-unit recording in the PNS, slanted 100-electrode microelectrode array from University of Utah were designed to facilitate contact with most of the nerve fascicles. Single unit activity was obtained in 10-20% of the electrodes and electrical depolarization was able to evoked graded recruitment of force in muscle groups in selective fashion (Branner and Normann 2000; Branner et al. 2001). However, insertion of these electrodes into the intact nerve caused mechanical damage, which limited their stability (Branner et al. 2004)(House et al. 2006; Polikov et al. 2006). In addition, these electrodes induce axonal compression and degenerating axons around the electrodes (Branner and Normann 2000). Furthermore, the mechanical rigidity of electrode material, electrode breakage and micromotions lead to secondary injuries thus increasing inflammatory response and adverse tissue reactions (Gonzalez and Rodriguez 1997), resulting in reduction of the recorded signal amplitude (Merrill and Tresco 2005).

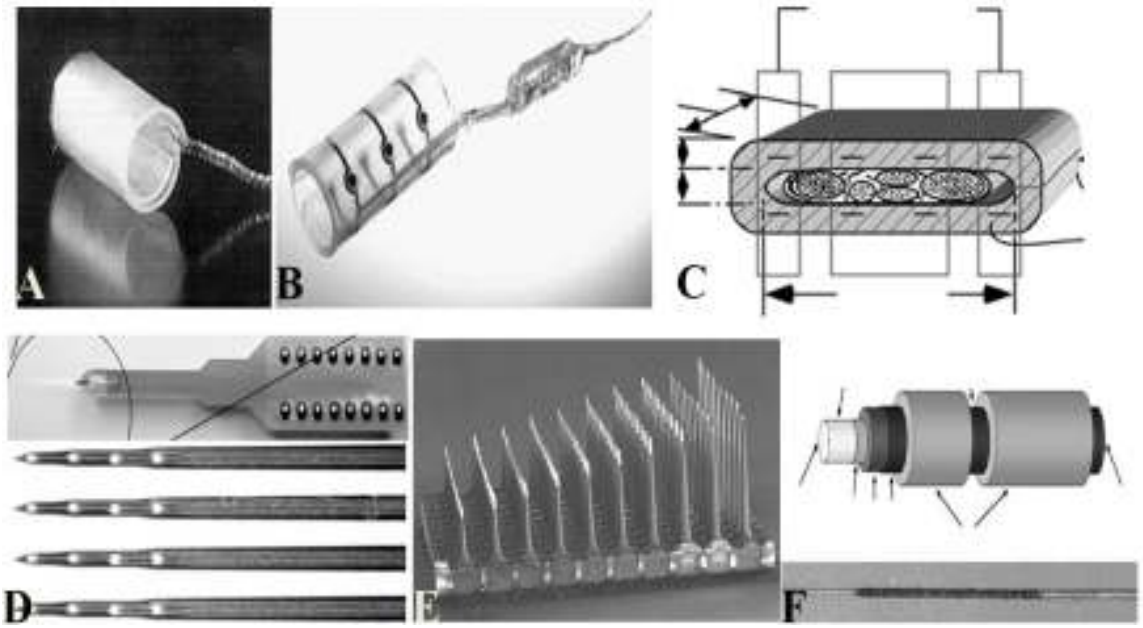

Figure 1.4: Epineural and intraneural electrodes used in peripheral neuroprostheses: A and B shows cuff electrodes made on silicone and hybrid silicone-polyimide respectively. C. Illustration of FINE electrode which gradually compresses the nerve to maximize recording/stimulation selectivity. D. SEM picture showing 16-channel Michigan probe. E. SEM picture of slant penetrating electrode developed at University of Utah. F. Schematic of LIFE electrode. All figures adapted from Navarro 2005.

1.2.7 Regenerative Interface

1.2.7.1 Regeneration of Nerve in Response to Axotomy

Unlike central nervous system whose axons degenerate resulting in permanent loss of nervous function after injury, peripheral nerves has a spontaneous regenerative capability (Gordon and Boyd 2003). Crush injury usually does not require synthetic guidance channels due to perseverance of epineurial and perineurial tubes to support axonal growth. But in case of third degree injury where there is disruption in all protective layers along with blood-nerve barrier, there is a need for bridge implants. After the peripheral nerve axotomy, distal portion of the nerve undergoes wallerian

degeneration in which cytoskeleton breakdown followed by cell membrane dissolution. Myelin debris at the distal portion is cleared by proliferating macrophages/ monocytes and Schwann cells. It has been shown that axonal membrane and myelin debris stimulate Schwann cell mitosis, and that macrophages that have phagocytosed myelin produce a conditioned medium that is mitogenic for Schwann cells (Baichwal et al. 1988; Fawcett and Keynes 1990). Activated Schwann cells then express regenerating associated proteins like laminin and fibronectin to increase the rate of extension and provide traction for neurons growing through the damaged region (Gilbert 2005). They also release appropriate cytokines and neurotrophins to support axonal regeneration and their reconnection to their targets (Schmidt and Leach 2003).

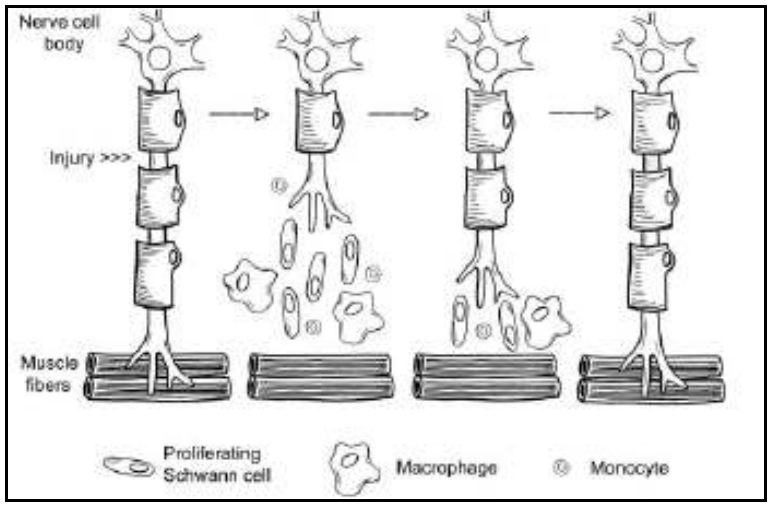

Figure 1.5 Peripheral nerve responses to axotomy: In the PNS, distal portion disintegrates after injury; proliferating Schwann cells, macrophages, and monocytes work together to remove myelin debris, release neurotrophins, and lead axons toward their synaptic targets, resulting in restored neuronal function. Figure adapted from Schmidt C, 2003.

1.2.7.2 Sieve Electrodes

Regenerative electrodes were developed to leverage the intrinsic property of injured peripheral nerve to regenerate spontaneously, the so called sieve electrodes consists of multiple Pt/Ir hole electrodes through which regenerating axons were induced to regrow (Edell 1986).

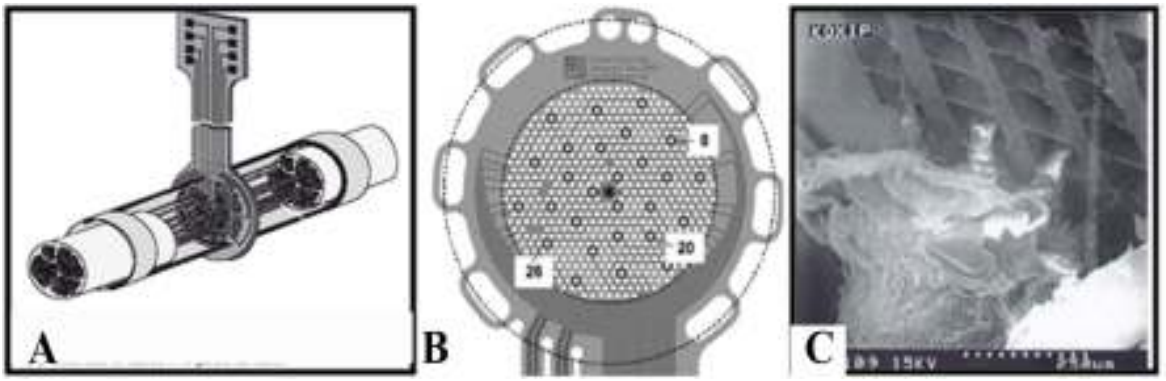

Figure 1.6: Schematic of regenerative sieve electrodes A. Schematic of regenerative interface where regenerating axons from transected nerve passes through via holes. B. Front view of sieve electrode consisting of via holes and electrode rings around them marked by black circles C. Constrictive axonopathy is seen near the electrode-tissue interface. (Navarro 2005; Lago 2007; Stieglitz 2002)

Using this electrode, neural activity was recorded from peripheral nerves of frog, rat and fish (Kovacs et al. 1992; Navarro et al. 1996) and facilitates selective stimulation of single axon or small fascicles. However these electrodes form a physical barrier to regeneration which limits the elongation of some of the sub-types of regenerating axons depending on size of via holes (Navarro et al. 2005; Navarro et al. 1996; Zhao et al. 1997). In addition, axons undergo constrictive axonopathy at the electrode interface as they start maturing and re-myelinating (Lago et al. 2005; Lago and Navarro 2007; Lago

et al. 2007a), where demyelination and neuronal degeneration was observed in distal regenerated axons in vicinity of the electrodes (Lago et al. 2007b).

1.3 General limitations

1.3.1 Metal electrode (safety vs sensitivity)

Most implantable metal electrodes have low charge transfer capacity and are inefficient to sense low amplitude signals due to its high impedance. In addition, the electrode selectivity (i.e. capacity to discriminate between individual neurons) is inversely proportional to the exposed metal surface. However, the electrode impedance increases proportionally to the reduced electrode area (Tykocinski 2001). Furthermore, insertion of these electrodes in nervous tissue leads to gliosis, acute inflammation, hemorrhages, and neuronal damage. These adverse tissue reactions like encapsulation and scarring forms a diffusive barrier which eventually mitigates the ability of the metal electrode to detect spiking activity (Merrill 2005). Since scar tissue acts as a mechanical as well as electrical insulator to soluble molecules and charged ions, it forces an increment in the stimulation threshold. However, large voltage can cause metal dissolution and the possibility of electrolytic tissue damage. Therefore, the need to create long-lasting sensitive and safe electrodes remains a challenge.

Current research aims at enhancing the quality of the neural interface by incorporating biological components like growth-promoting factors to entice axonal sprouting on the recording surface or anti-inflammatory drugs to reduce inflammation (Campbell et al. 1991; Pettingill et al. 2007; Rejali et al. 2007; Yamagata et al. 2004), improving the electrochemical characteristics of the probe through advanced coatings

(Ludwig et al. 2006; Richardson et al. 2007; Wang et al. 2006) and developing integrated electronics for wireless communication to the external devices (Ghovanloo and Najafi 2007).

1.3.2 Recording/stimulation of mixed modality nerves

Peripheral nerves consists of different kinds of fibers classified based on their function (motor or sensory) and conduction velocity (large myelinated A fibers, pain C fibers etc). When recording from a mixed nerve, the identification of neural signals is done using spike sorting techniques, principal component analysis, interpolation, cluster analysis, and filter based methods (Lewicki 1998). However, the identification of those from specific neuronal sub-types is not currently feasible. In addition, the perception of small receptive fields is dependent on the ability to stimulate only a small number of sensory axons (Riso 1999), and stimulation with multielectrode arrays inserted into the mixed nerve leads to perception in large receptive field. Furthermore, the non specific stimulation a mixed nerve triggers sensory-motor depolarization and thus undesired sensations and movements. Thus, axon-type specific regeneration and segregation might be required to facilitate modality-specific stimulation.

1.4 Specific aims of the project

The making of a revolutionized prosthetic limb demands the creation of an advanced neural interface that overcomes specific challenges that limit neural control and natural sensation of the robotic prosthesis. The general aim of this study is to enhance the stability of neural interface and ultimately increase the functional efficiency and longevity of the prosthetic device. We specifically sought to:

1. Achieve regenerative neurointerfacing through multielectrode arrays of open architecture.
2. Induced modality specific axonal regeneration from a mixed neuronal population.
3. Enhance the sensitivity of the implantable electrodes by the use of conductive nanomaterials.

CHAPTER 2

REGENERATIVE NEUROINTERFACING THOUGTH MULTIELECTRODE ARRAYS OF OPEN ARCHITECTURE

2.1 Background

Multi-electrode arrays inserted into the nerve causes mechanical injuries and axonal compression leading to immunological response consisting of macrophages activation and infiltration. Chronically, such inflammation is characterized by foreign body giant cells formed by the fusion of macrophages and monocytes (Anderson et al, 2008). Subsequently, there is infiltration of fibroblasts and neovascularization at site of injury which isolates the implant via fibrous encapsulation (Anderson et al. 2008), thus contributing to the eventual loss of neural activity recordings (Szarowski 2003). Sieve electrodes consisting of electrode holes are spatially constrictive and hamper the normal regeneration process due to its closed architecture. In this study, we evaluated nerve regeneration through multielectrode array of open architecture which is anticipated to avoid interfering with the nerve regenerative process and facilitate stable tissue-electrode integration. Evaluation of nerve regeneration was done in acute and chronically injured animals which mimics the physiological condition of the amputee.

2.2 Methods

2.2.1 Electrode-Conduit Assembly

Floating microelectrode array consisting of 18 platinum/iridium microwire electrodes, insulated with parylene-C with the impedance values ranging from 150K-

250KΩ at 1 KHz (biological relevant frequency) were purchased from Microprobes Inc, MD (shown in subset of Fig2.1C). These electrodes were custom made to have different heights (0.5-0.9 mm) with a separation of 400µm between them to maximize the contact with regenerating axons. A 250µm thick alumina ceramic base plate holding the electrodes was fitted onto the polyurethane tubing to form a regenerative interface. To facilitate electrophysiological recordings, the flexible gold wires from the base plate were connected to the metallic headcap which consists of 18-pin female omnetics connector sealed within the case with Epoxy. The entire assembly was sterilized and filled with collagen one day prior to surgery and then filled with collagen (Fig 2.1C).

2.2.2 Animal Preparation and Electrode Implantation

All the animal care and surgical procedures were performed in accordance to Institutional Animal Care and Use Committee (IACUC) of UT Southwestern Medical Center, Dallas. A total of 10 adult lewis rats, weighing from 150-250 kg were used in this experiment. Rats were anesthetized with ketamine/medetomidine (87 mg/kg). Animals head and left thigh region was shaven and skin was disinfected with butadiene and isopropanol in scrubbing motion. Eyes were kept moist with ophthalmic ointment and temperature was monitored during the surgery. Figure 2.1D shows schematic of surgical procedure where rostro-caudal incision of half inch was done on the dorsal aspect of the head to mount headcap using dental cement as shown in Fig 2.1A. Lead wires connecting metallic headcap to the electrode array were passed subcutaneously to the incised anterior edge of the biceps femoris muscle. The fascia overlying the muscle was incised and muscle was reflected to expose the sciatic nerve. The nerve was then transected above the

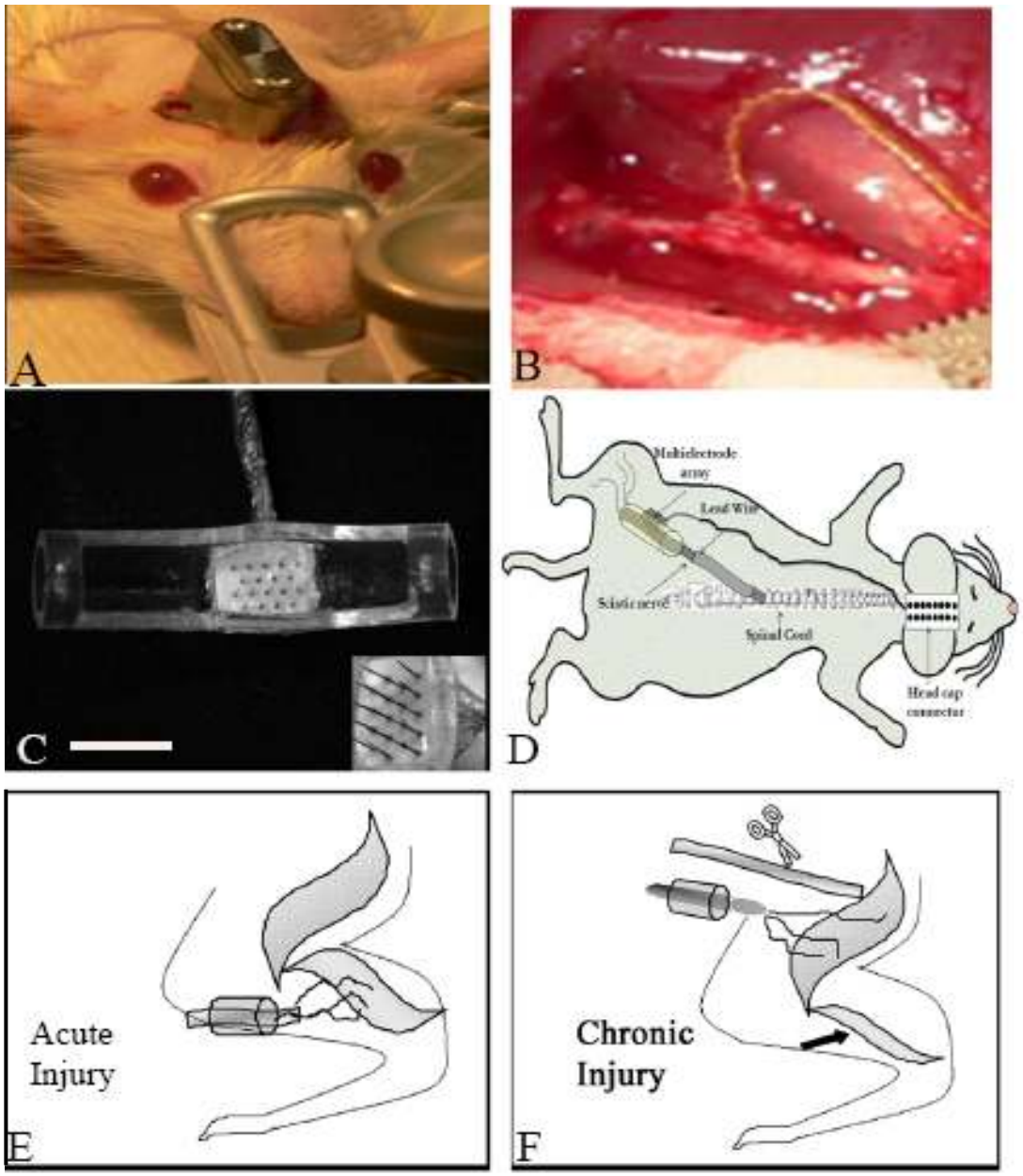

Figure 2.1: Multi-electrode array in regenerative paradigm**:** A shows headcap implantation on the rat cranium. B shows the ends of transected sciatic nerve sutured to the nerve guide tube mounted with the electrode array. C. Light micrograph showing top view of 18 electrode array mounted in a microrenathane based nerve-guide tube. D: Schematic of entire surgical procedure is shown where electrodes were placed in sciatic nerve and interconnecting lead wire is passed subcutaneously. Schematic of acute injury model is shown in E whereas F shows a chronic injury model. Scale bar (C) = 2mm.

bifurcation point, its proximal and distal ends were introduced into opposite ends of the conduits securing it with 10-0 ethylon suture to facilitate end-to-end repair seen in 2.1B. The fascia and the skin were closed in layers with resorbable (6-0 chromic gut) and non-resorbable (6-0 silk suture) sutures respectively. At the completion of the surgery, antipamezole (1mg/ml) was used to retrieve animal from the anesthetic condition. Study was performed in two injury models- acute and chronic injury models. In acute injury model, nerve was transected followed by immediate electrode implantation as schematically described in 2.1E; whereas in chronic injury group, following the nerve transection, proximal end was sutured to the adjacent muscle. Approximately after six months of injury, procedure similar to acute implantation was done as shown in 2.1F. Post operative care included oral doses of thimerosal (TMS), subcutaneous injection of bruprenex and topical application of bitter end. Conventional chip bedding was replaced by cellu-dri bedding to prevent mechanical injury to the animals. Animals were kept in humidity/temperature controlled room with 12 hour light/dark cycle with constant supply for chow-chow and water.

2.2.3 Sample preparation

After the completion of survival period, perfusion was done with saline followed by 4% paraformaldehyde (PFA). The implant was harvested and the regenerated tissue was carefully isolated from the electrode array. Further, tissue was fixed overnight in 4% PFA. The proximal and distal nerve ends were marked with a dye and then embedded longitudinally in paraffin wax for further processing. The horizontal and coronal

(represented by a and b respectively in Fig 2.2A) paraffin sections of 6μm thickness were obtained and mounted onto capillary-gap charged slides (lilac-Fisher).

2.2.4 Immunohistochemical analysis

Sections were deparaffinized with three changes of xylene followed by re-hydration in descending grade alcohol and then wash with distilled water. Then the sections were blocked with endogenous peroxidase with 3% H_2O_2 in distilled water followed by universal blocking agent. Sections were then washed, incubated in primary followed by secondary antibodies. Primary antibodies used: S100 (for Schwann cells, 1:300 dilution, polyclonal rabbit anti-cow- DAKO Z0311); Mouse anti-200 KD neurofilament protein (for axonal profiles 1:300 dilution- Dako M0762); mouse anti-ED1 (for activated macrophages; 1:50 dilution-Chemicon); mAB MBP (for myelination). DAB solution was used as a substrate. Hematoxylin treatment followed by ammonia water was used as a counter-stain.

2.2.5 Immunofluorescence staining

Paraffin sections were deparaffinized with 3 changes of xylene, rehydrated in descending grade alcohol and then washed in distilled water. Sections were blocked with 5% normal goat serum (GIBCO) mixed in 1% triton X-100 (Sigma) made in phosphate buffered saline (PBS) for one hour at room temperature followed by overnight application of primary antibodies diluted in blocking buffer at 4^oC. The following day, sections were washed and secondary antibodies were applied for two hours at room temperature. Mounting was done using vectashield containing DAPI (Vector Labs, CA) to stain nucleus. All the primary antibodies were purchased from Chemicon, Temecula,

CA and secondary antibodies from Jackson ImmunoResearch Laboratories, West Grove, PA.

Table 2.1 List of antibodies used with their concentrations

Antigen	Tissue specificity	Primary Concentration	Secondary Concentration
Neurofilament protein (rabbit anti-NFP)/ ED-1(mouse anti-ED1)	Axonal profiles/ activated macrophages	1:100/1:500	1:250/1:500
B-tubulin (mouse anti b-tub/S100 (rabbit anti-S100)	Axonal profiles/ Schwann cells	1:50/1:250	1:400/1:500
Myelin Basic Protein (rat anti-MBP) /ED-1 (mouse anti-ED1)	Myelinated axons/activated macrophages	1:50/1:500	1:400/1:500
Myelin Basic Protein (rat anti-MBP)/ calcitonin gene related peptide (rabbit anti-CGRP	Myelinated axons/ trkA+ pain fibers	1:50/1:1000	1:400/1:1500

2.2.6 Electrophysiological studies

The neural data acquisition system (PBX216WB450 2005, Plexon, Dallas, TX) was used to record neural activity from regenerating axons in a freely moving animal every week. This 16-channel recorder has a theoretical capacity to record from 64 neurons simultaneously i.e. four per channel at 25 second precision. Signals from the head stage consisting of field effect transistors (FET) with unity gain were routed by bus connector to be amplified and digitized by Plexon's data acquisition unit. By visual inspection of analog signal on oscilloscope (Tektronix, DSA 8200) and digitized signal on the recorder program (library 6.5, driver 7.4.0), voltage threshold was set. Only those events which crossed the set threshold were recorded and further processed using a data offline spike sorter program (OFSS, Plexon). Three component principal component

analysis (PCA) was used to isolate single units from the noise (Chapin 2004; Nicolelis and Ribeiro 2002). All the channels had independent control over gain, filter frequency cut-offs and reference to maximize the extraction of information from the neuronal activity.

2.2.7 Behavioral studies

Nociceptive recovery in rats with chronic and acute axotomy was evaluated by eliciting pain in response to thermal stimuli using plantar heat equipment (Ugo Basile, Varese, Italy). Animals were placed in a plexiglass chamber and allowed to stabilize for 15 minutes before applying the heat stimulus. Source of infrared beam was positioned under the plantar surface of the hind paw and a photocell (7370-372EW01) detects time from which the heat stimulus is applied until paw withdrawal. This time period was marked as paw withdrawal latency (PWL) that indicates the nociceptive threshold with 0.1 sec precision. Second reading for the same paw was not tested within an interval of 10 minutes to avoid response due to anticipation (Romero et al. 2007). Also tactile perception recovery was evaluated in the paw using a anesthesiometer (Ugo Basile, Varese, Italy), in which a gradient force is applied by a filament to the paw. Force and time after which paw was withdrawn was noted.

Motor function recovery was evaluated in a rat sciatic nerve model by using toe spread assay. It is a natural instinct of an animal to stretch its toe when it is suddenly lifted up. Images of the injured left and normal right paw for all the rats were captured using camera (Panasonic, AG-EZ30) from a fixed distance when the rat was lifted up.

Toe spread index was calculated by taking ratio of distances between the first and fifth toes of injured to non-injured leg.

2.2.8 Imaging and quantification

Quantification of proximity of the NFP+ regenerated axons from the active site was done using Axiovision application (Carl Zeiss, Axiocam, version 5.07.03). Light micrographs of all tissue-electrode interfaces of horizontal view were obtained and distance between axon and electrode edge was measured. For quantifying the extent of inflammation for each animal in a group, light micrographs of all electrode interfaces were obtained and spatial distribution of ED1 immunoreactive region was measured in four different areas A, B, C and D (shown in Fig 2.2B).

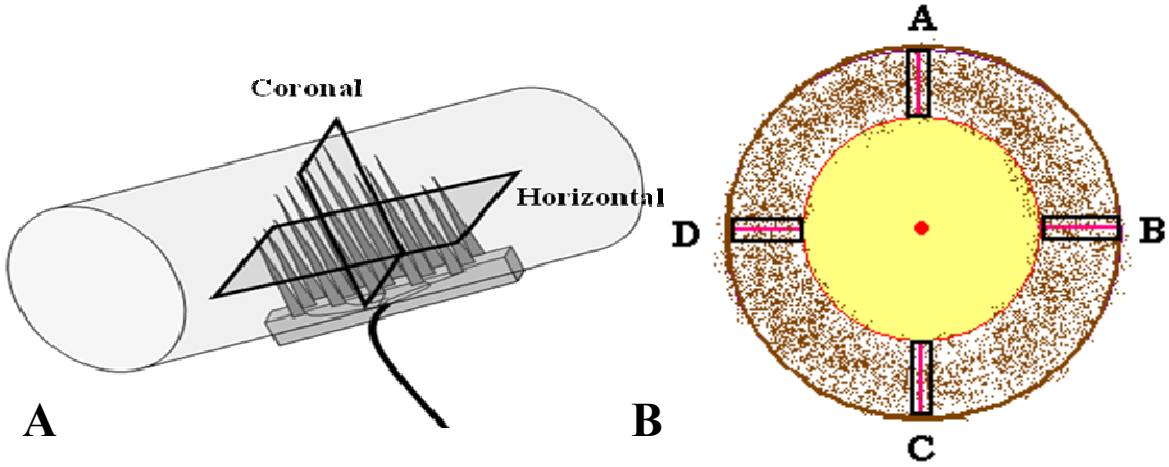

Figure 2.2: Method for quantifying extent of inflammation: A shows the schematic of electrode-conduit assembly with planes of sectioning; B is a schematic of a tissue-electrode interface (yellow-electrode; brown-macrophages). Axial immunoreactivity was quantified by measuring the lengths of positive stained areas in four directions.

Carl Zeiss 510 laser scanning microscope was used to take low and high magnification pictures for immunofluorescent studies, with the probe-site centered in the field. Quantification of the fiber growth in proximal, middle and distal portion of the

regenerated tissue in each of the animal was done using LSM510 image examiner software (Carl Zeiss, version 3,2,0,115). Optical densitometry method was used in which double-level thresholding to eliminate saturation and background was done (Romero et al. 2007; Romero et al. 2001). Then the boundaries of positively stained area were marked and the total area in square micrometers, consisting of density profiles lying within cut-off window was measured.

2.2.9 Morphological Analysis of Muscle

Gastrocnemius muscle from experimental and unoperated leg was harvested and their fresh weight was measured. The tissue was then snap- frozen in iso-pentane pre-cooled in liquid nitrogen to -160^{o}C. Cross sections (10µm) were then stained for acetocholinesterase receptors at neuromuscular junctions using non-specific esterase method (Stoward 1991). This method works under principle of hydrolysis of naphthol derivatives (alpha-naphthyl acetate) and utilization of azo dye (hexazotised parasosaniline) which acts as capture agent to produce insoluble products at the site of enzyme activity. Briefly, slides were incubated in NSE incubation media made of mixture of NSE substrate solution, hexazotised pararosaniline and phosphate buffer for 40 minutes at 37^{o}C. Slides were then washed in running water for 10 minutes, dehydrated in ascending grade alcohol and then mounted with cytoseal (TSRH manual, policy no CPH-016).

2.2.10 Statistical Analysis

All tissue-related data is reported as the mean±standard deviation and mean±standard error of the mean (SEM). An unpaired two-factor student's t-test for

unequal variances was used to determine statistical difference between two means. p values less than 0.05 were considered to be significant.

2.3 Results

Eight of ten rats survived the surgery and remained healthy throughout the study. No signs of self-mutilation of the hind limbs were observed in any of the animals after the nerve gap repair surgery.

2.3.1 Evaluation of regenerating axons through the electrodes

Regenerated nerve covered the entire lumen of the conduit as shown in 2.3A. This was typical for most cases except for two where regenerated tissue was found covering only the electrode area. In all the harvested implants, regenerative conduits were covered by vascularized fibrous tissue. Robust nerve regeneration was observed in both the acute and chronic injury groups with 10-12 electrodes in contact with regenerated neural tissue. Regenerated neural tissue covered the entire shank of the electrode. Tissue-electrode interfaces which appeared after removal of the electrodes from the regenerated tissue are shown in Fig 2.3B harvested from an acute injury animal with 19 days of implantation. To distinguish between region of scarring, connective tissue encapsulation, inflammatory region, necrosis or apoptosis also to study various cell interactions around the foreign implant, histochemical analysis was performed. Regenerated axons positively marked by neurofilament protein were found to be in close proximity to the electrodes. (approximately 10-150 μm) in both the experimental groups. The electrodes did not seem to obstruct the regenerating axons. Fig 2.3 shows immunoreactive regions for neurofilament after immunoperoxidase staining in acute injury group (C-low and D-high

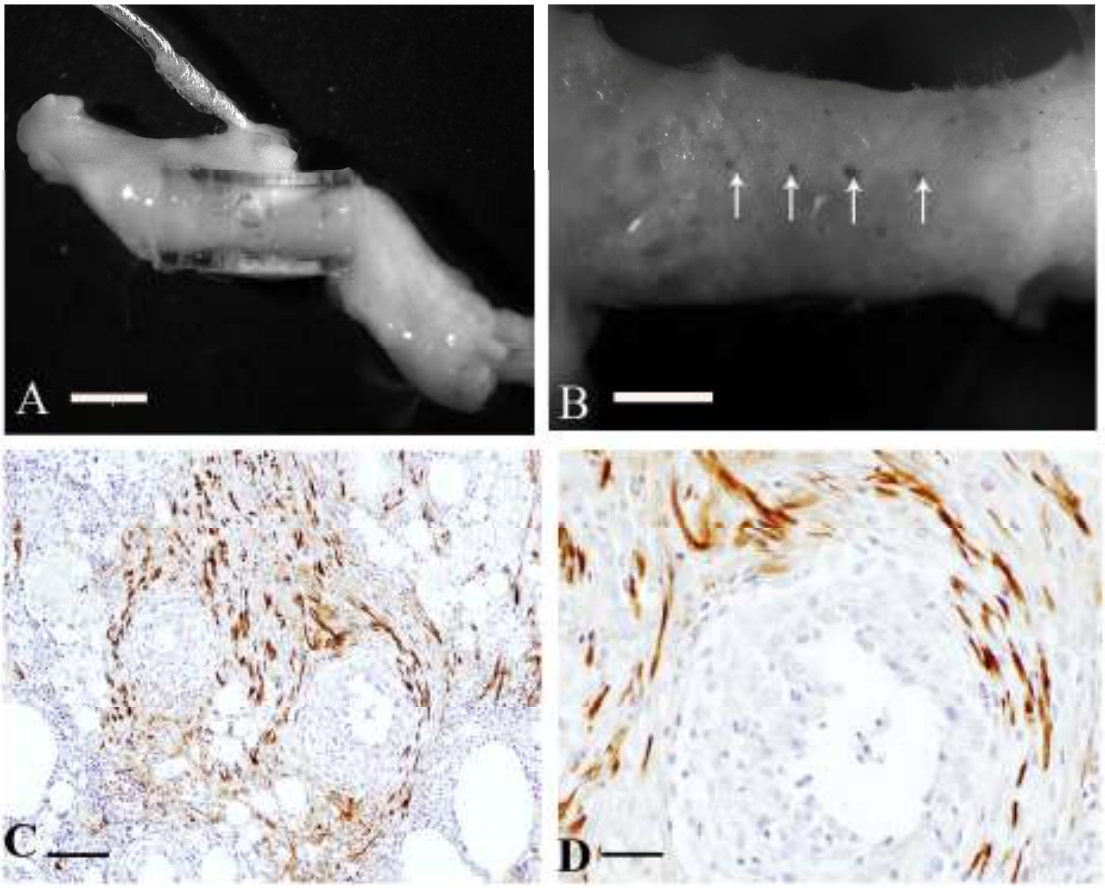

Figure 2.3: Robust axonal regeneration around the electrodes is demonstrated: Gross anatomical picture of regenerated nerve within the electrode-conduit assembly in case of acute end-to-end repair is shown in A. B shows a light micrograph of regenerated tissue detached from the conduit where white arrows are pointed towards the tissue-electrode interfaces. Low (C) and high (D) magnification light micrograph shows positive immunoreactivity for neurofilament 200KDa, a specific marker for axons indicated by the dark brown regions in close vicinity to the electrode site in case acute injury group. Asterisk represents the position of the electrode. Scale bars= 2.5 mm in A, 1mm in B, 100µm in C and E; and 30 µm in D and F.

magnification). However meticulous quantification of proximity of axons from the periphery of the electrodes indicated that axons were closer to the electrodes in case of acute injury group (12.13±3.03 µm) compared to chronic injury group (28.28±12.18 µm) with the statistical significance of $p<0.001$. One animal from the acute injury group was eliminated from the above quantification since it had significantly larger distances

between its axons and the active surface due to the least survival period of 19 days. This is a valid elimination since maximum inflammatory response is observed after two weeks (Leung et al. 2008) which tends to push away the regenerated axons farther away from the recording surface thus increasing the measured values. Thus this animal was considered to be the outlier in this case.

2.3.2 Myelination of regenerated axons

Tissue sections were further stained for S100 protein, normally present on the Schwann cells to confirm its presence near the interface and were found to be in the direction of axonal growth as shown in Fig 2.4A&B. Fig 2.4C&D shows representative confocal image from acute injury group double-labeled for Schwann cells (red, marked by S100) and axons labeled by β-tubulin (green). Glial cells were found to be in close association with axons and some extent of co-localization indicates myelination of the regenerated axons.

Regenerated tissue was further stained for markers for different sub-types of axons i.e. myelin basic protein which is a specific marker for all the myelinated axons (red, Fig 2.4E) and calcitonin gene related peptide which is a specific marker for unmyelinated axons, a subset of sensory axons (green, Fig 2.4F). It was observed that both large diameter myelinated as well as small diameter non-myelinated fibers had successfully regenerated through the multi-electrode pins. Myelinated axons could comprise of motor and proprioceptive axons whereas axons marked by CGRP are only trkA+ nociceptive pain fibers. Unlike seen in sieve electrodes which is spatially constrictive, regeneration of large diameter myelinated axons in our approach was not

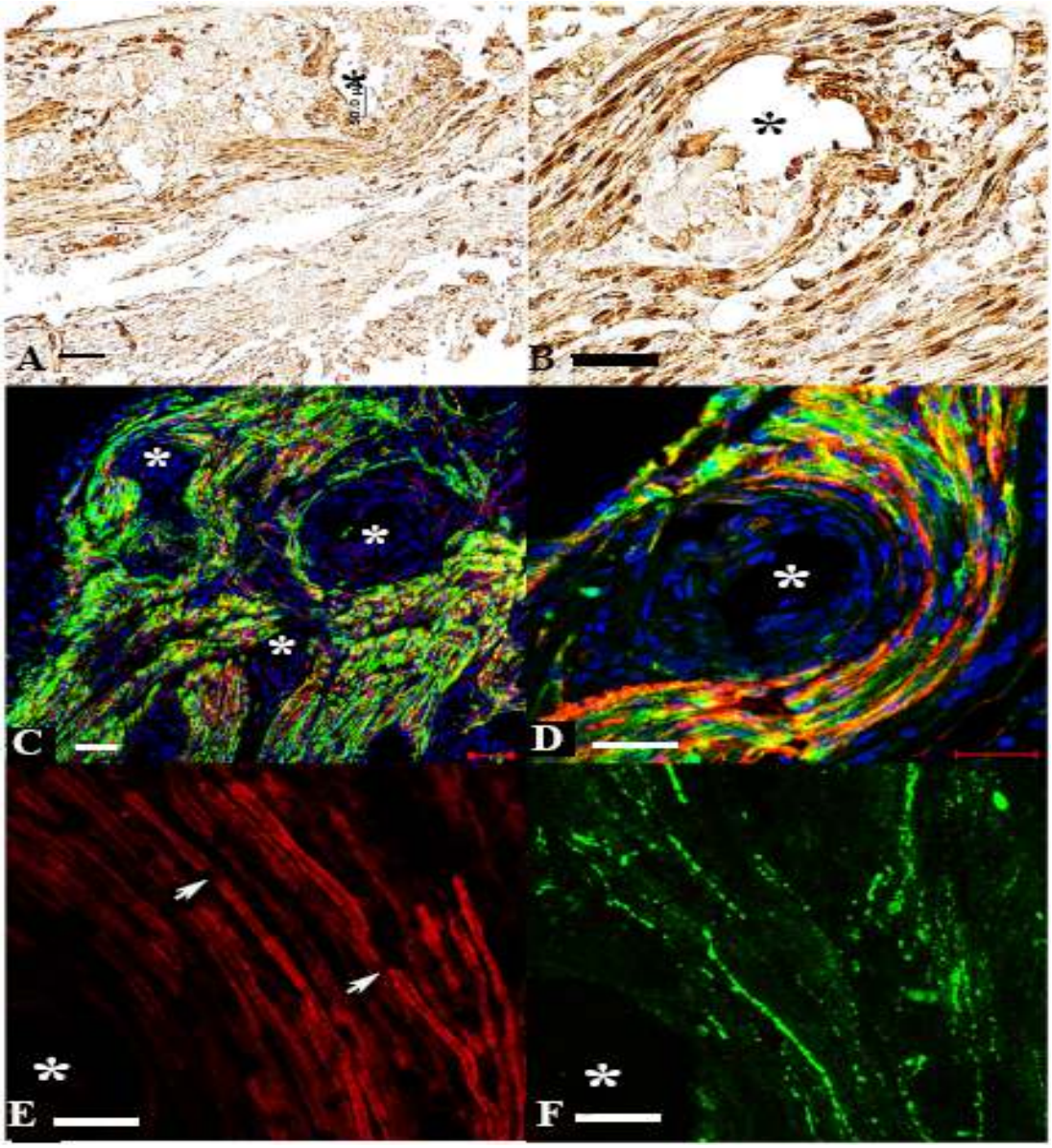

Figure 2.4: Regeneration of myelinated and unmyelinated axons: A&B: Presence of Schwann cells marked by S100 was noted by positive dark brown staining around the electrode. C&D shows tissue section double-stained for S100 (red) and b-tubulin (green) where co-localization of both immunoreactive regions (yellow region) indicates myelination of axons. Both myelinated (E, labeled by MBP-red) as well as non-myelinated axons (F, labeled by CGRP-green) had successfully regenerated through the electrode array. Center of the electrode is marked by asterisk. Scale bars=50µm in B,D,E,F and 100µm in E,F.

hampered. Nodes of ranvier were seen close to the electrode surface marked by the white arrows in Fig 2.4E indicating that the myelination was normal.

2.3.3 Extent of Inflammation around the electrodes

It was observed that some areas near the electrode surface were absent of axonal as well as glial profiles, suggesting some degree of tissue reactions to the foreign body (Fig. 2.4 C-D). Further labeling for reactive macrophages revealed their presence in close proximity to the electrode in both the groups. The accumulation of macrophages was minimal i.e. limited to 2-4 cell layers and highly localized to bio-abio interface. Fig 2.5 shows low and high magnification light micrographs for coronal section (A- low magnification, B-high magnification) and horizontal sections (C, D) stained using indirect immunoperoxidase technique. Quantification of the inflammation area determined by the length of ED-1 immunoreactivity from the electrode surface to the last positive cell in cross section revealed larger inflammation around the electrodes in chronically injured animals (30 ± 10 μm) as compared to those implanted at time of surgery (20 ± 5 μm) as shown in Fig 2.6. This increase is equivalent to additional 1-3 cell layers in chronically injured animals. Extent of inflammation was homogenous in all the animals, though the immunoreactive extent varied within the same section. Fig 2.7 shows that increase in the inflammation in chronic group is statistically significant ($p \leq 0.01$) as compared to acute injury group.

2.3.4 Effects of macrophages presence on surrounding tissue

To evaluate the possibility that the macrophage coating of the electrodes was protective or reactive in nature, tissue was double-labeled with neurofilament protein,

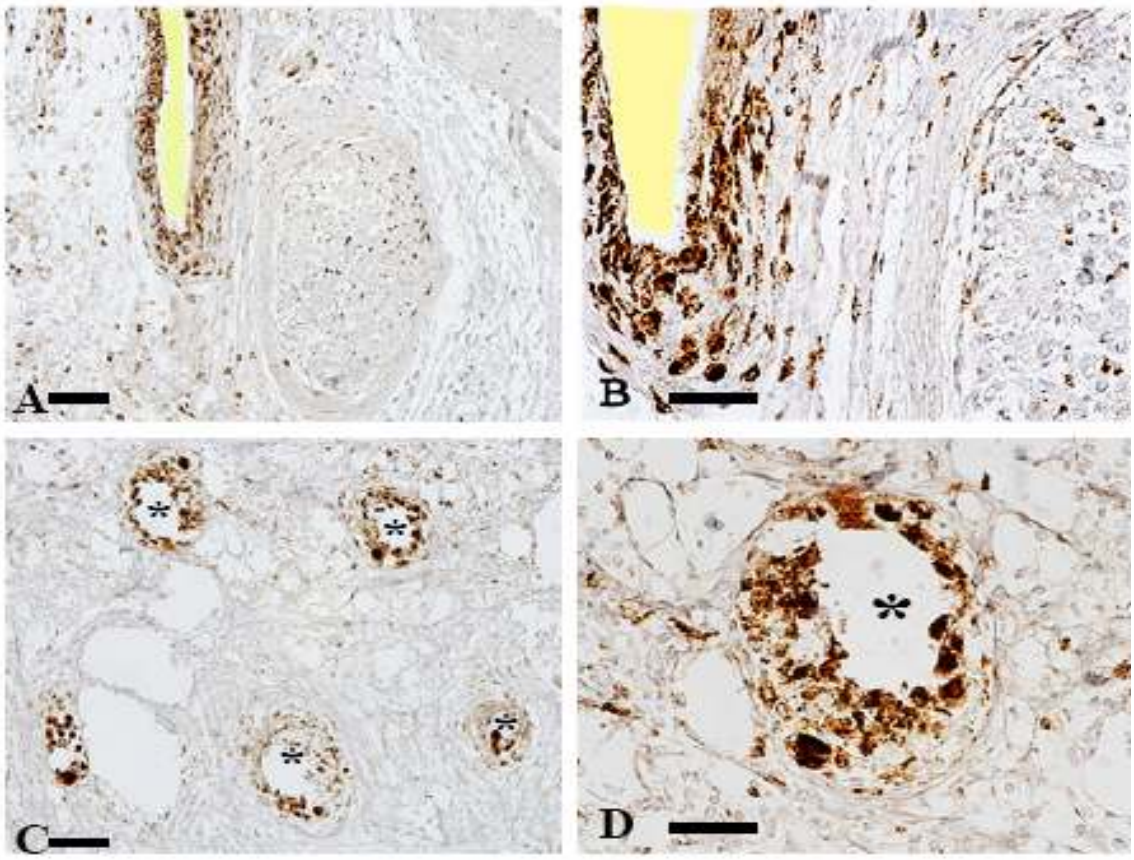

Figure 2.5: Intimate contact of macrophages to the electrodes: Low (A, C) and high (B, D) magnification pictures shows electrode-tissue interface in coronal view, section along the electrode tract in A&B and horizontal plane perpendicular to the tract (C, D) stained for ED-1 antigen present on activated rat macrophages (brown color). These images indicate minimal inflammation restricted at the interface (3-4 cell layers). Scale bars= 50μm in B, D and 100μm in A, C.

specific marker for axon (green) and ED-1, antigen on reactive macrophages (red). The representative pictures showed in Fig 2.8A&C shows the comparison of inflammatory response and corresponding presence of regenerated axons in both the experimental activated macrophages indicating inability of the regenerating axons to grow in that region. This could be due to toxic environment produced by macrophages or alteration in the extracellular environment near nerve-electrode interface. The probable cause for the

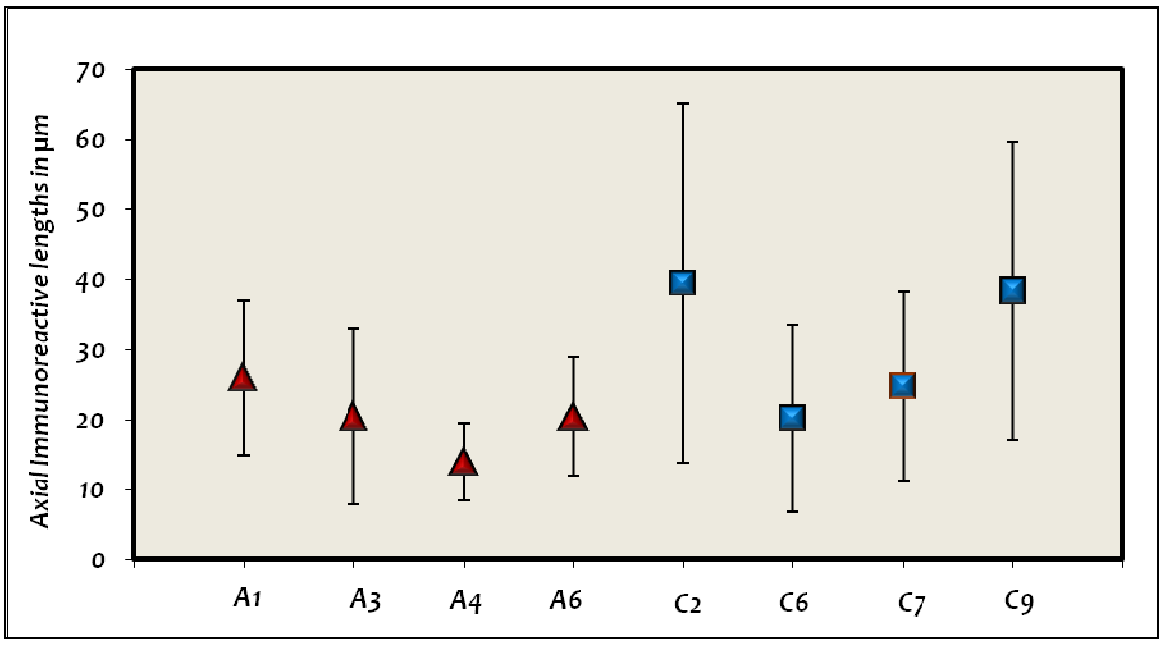

Figure 2.6 Quantification of axial immunoreactivity of ED-1+ cells: The mean axial immunoreactive length indicating spatial distribution of positively stained macrophages at the tissue-electrode interface is plotted for each of the animal. On average, limited and homogenous coating was observed in both the groups with the variability ranging from 10µm to 65µm.

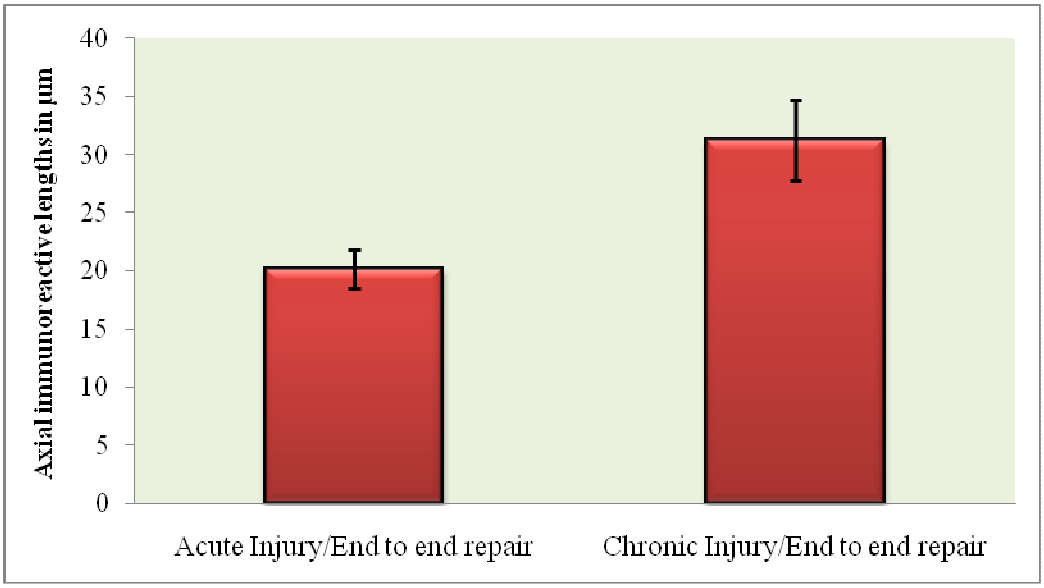

Figure 2.7 Increased inflammation in chronically injured animals: Above figure shows that the inflammatory response in the chronically injured animals was significantly higher ($p \leq 0.01$) than acute injury group.

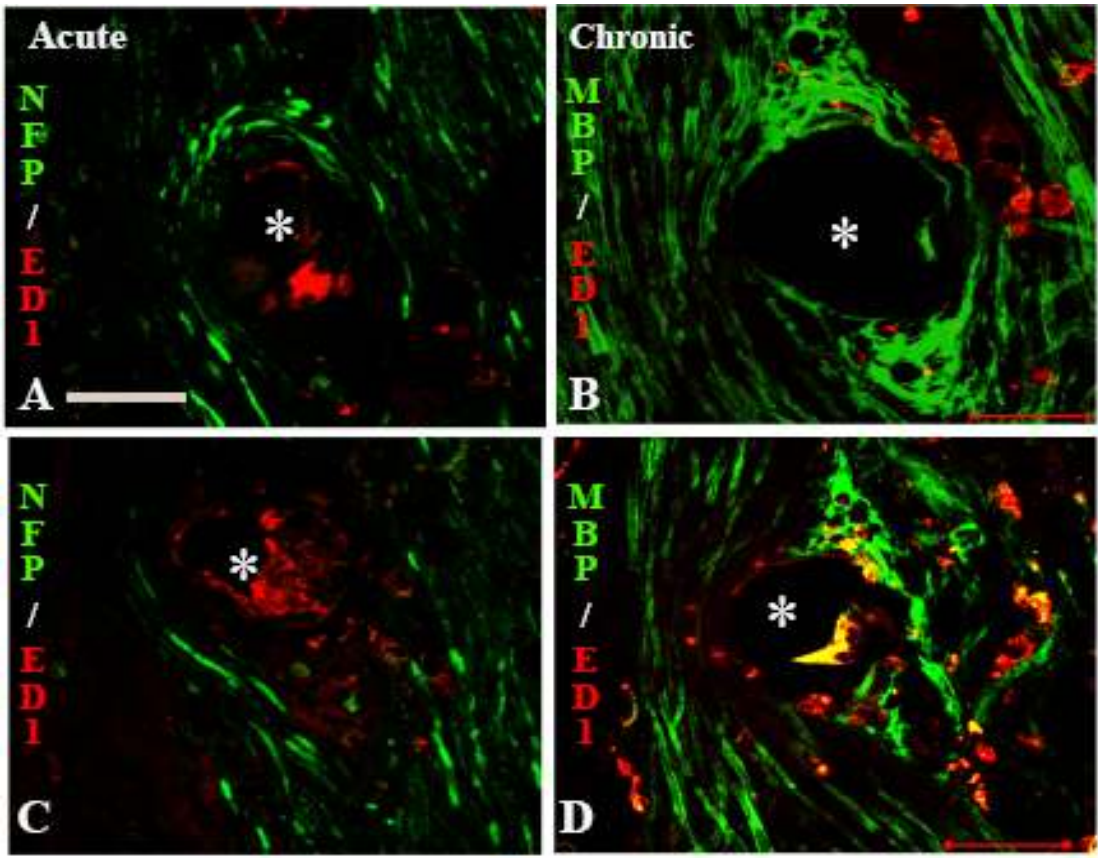

Figure 2.8: Effects of macrophages on surrounding tissue: Confocal micrographs of transversely cut sections of the nerve regenerated through the multielectrode array implanted at the time of injury (A, B) and after 6 months of nerve amputation (B, C), showed axons (A, C; NFP+; green) and re-myelination (B, D; MBP+; green) to occur in the presence of a limited number of activated macrophages (ED-1+; red) at the tissue-electrode interface. Also increased ED1+ spatial and temporal reactivity was observed in chronic (C,D) as compared to acute injury animals (A,B). Scale (A-D) = 50µm.

groups. Inverse proportionality is observed in areas containing regenerated axons and increased inflammation in case of chronics (2.8C-D) is the fact that the trauma to the nerve before the implantation surgery could have led to increased presence of resident macrophages in surrounding tissue as compared to that of acute injury group in addition to the ones which are infiltrated during regeneration. To study effect of macrophages on myelination, double labeling was done using MBP (green; marker for myelination) and ED1, antigen on macrophages (red). No signs of degenerating axons (2.8A, C) or affected

myelination (2.8B, D) was observed in close vicinity to macrophages indicates protective role of these cells.

2.3.5 Variation in regenerating capacity of acute and chronically injured sciatic nerve

Immunolabeling of the specific neuronal marker β-tubulin (green) at proximal, middle, and distal levels of the regenerated tissue from animals implanted at the time of injury (Fig. 2.9 D-F), or after chronic nerve amputation (Fig 2.9 J-L), demonstrated the presence of abundant regenerated axons at the middle of the electrode array and into the distal nerve stump, demonstrating that regenerating axons successfully transverse the multi-electrode array placed in the lumen of the nerve guide. There was more reduction in total axonal growth in distal portion of regenerated tissue of chronically injured nerve (n=3) as compared to acute injury group (n=2), thus indicating difference in their regenerative capacity as per data shown in table 2.2. It was also observed that amount of inflammatory response differs along the length of the same regenerated tissue as shown in Fig 2.9 i.e. in proximal, middle and distal regions of the transected nerve. Least inflammatory response was observed near proximal region, with localized response around electrodes and elevated response in distal regions. Following table shows the percent axonal growth (area in μm^2) in middle and distal regions with respect to the total axonal growth in proximal region.

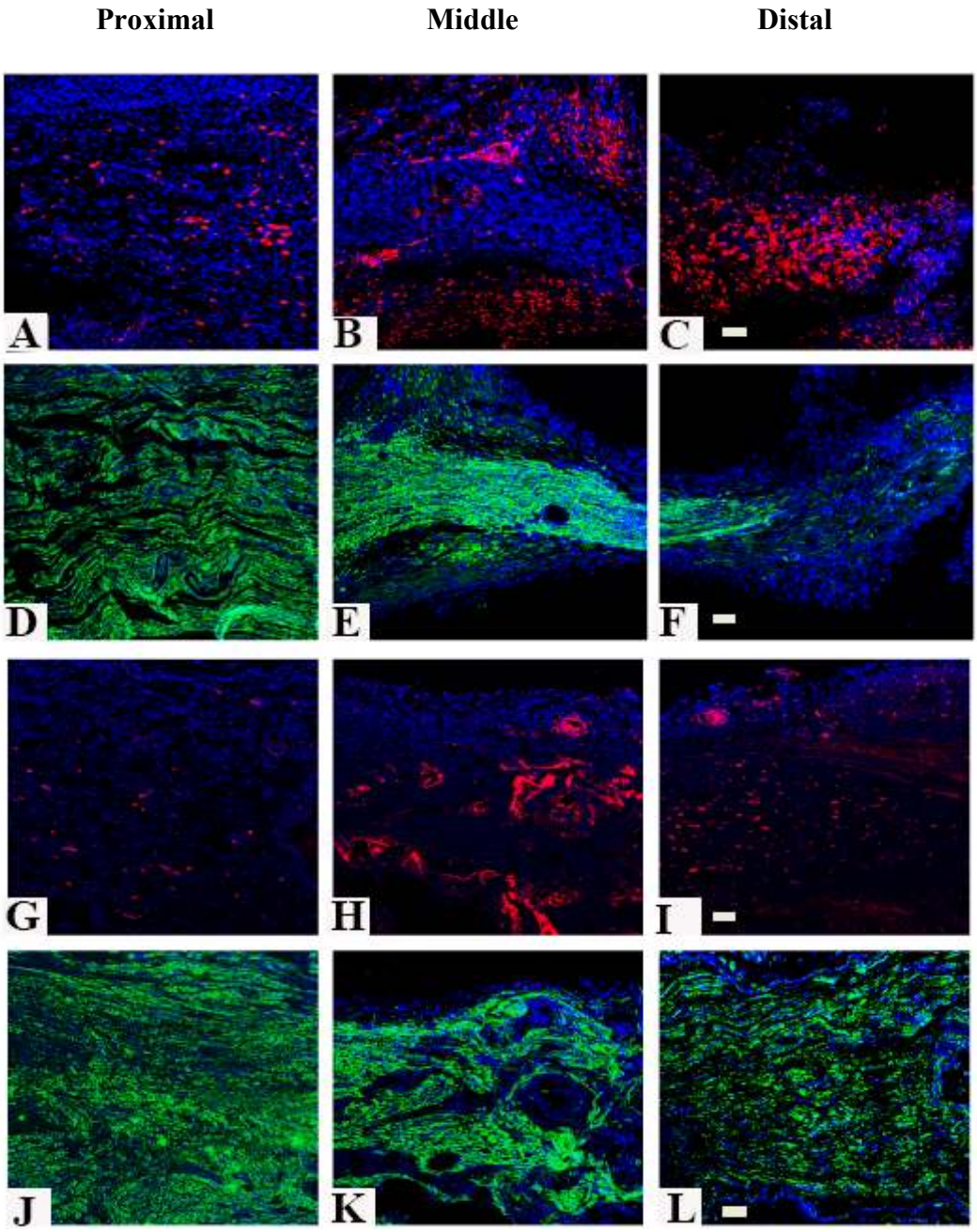

Figure 2.9: Variability in regenerative capacity of acute and chronically transected nerve: Above figure shows the immunofluorescence images of proximal (A, D, G, J) middle (B, E, H, K) and distal (C, F, I, L) region of the regenerated tissue. Tissue is stained for activated macrophages labeled in red and axons (green) to see variability in axonal regeneration and extent of inflammation in these three regions. A-F show representative pictures of chronically injured animal whereas G-L shows images from acute group. Inverse proportionality between both immunoreactive areas holds true.

Table 2.2: Total axonal growth of acute and chronically injured nerves based on axonal density in proximal portion

Experimental groups	Middle region (% proximal)	Distal region (% proximal)
Acute Injury	94.92 ± 34.7	48.07 ± 7.8
Chronic injury	56.88 ± 4.2	26.96 ± 6.7

2.3.6 Functional Assessment of Nerve Physiology

We successfully recorded from 6/8 animals and were able to detect neural activity approximately on 80% of the total active sites and in some cases for more than two months post implantation. However, due to the complexity of the experimental paradigm and technical difficulties faced like splintering of lead wire at anatomical joints and tethering forces, we were unable to record for more than three months of implantation. In our recordings, the SNR was 7:1 with spike amplitudes ranging from 100μV to 850μV. The earliest detection of neural activity was obtained at 8 days post implantation from the animal with chronic injury of 203 days and was persistent up to two months post implantation.

This study was done to evaluate ability of this interface to detect neural activity generated by adjacent neurons; thus recordings were not correlated to the behavioral changes. Representative image in 2.10 shows single unit (A) and multi-unit activity (E) isolated from recordings taken from regenerated axons chronically injured for 223 days, 8 days post implantation. 5/16 electrodes had total of 7 units with typical extracellular signal shapes out of which two had multi-unit detection. D&F shows clusters in distinct

3D spatial distribution represented by their respective color in a principal component analysis (PCA) plot. The clustering as well as waveform contouring method was used to isolate the units from raw data. The variability within the firing of the above marked units is shown in C and G respectively with the mean marked by the solid line and limits of the range indicated with dotted line. When the same rat was recorded 12 days later at 20 days post-implant, single unit activity was observed at 9 separate electrodes.

Figure 2.11 shows changes in the unit amplitude in one of the examples the electrodes monitored over time as the nerve undergoes the process of regeneration and re-myelination over time. Representative image shows one of the electrodes which initially had multiple unit detection lost one unit over time. After 8 days of nerve regeneration, 5/16 electrodes had single and multi-unit activity, but after 46 days post implantation 9/16 electrodes had single unit activity. This increasing trend in number of active recording sites was likely due to increasing number of regenerated axons in close proximity of electrodes. These results demonstrate that sciatic nerve regeneration suggested by the physical and histological findings includes signs of neural activity. This unit activity though changes in its attributes, was sustained during longer periods of time.

2.3.7 Assessment of functional Recovery

The robust regeneration was obtained through the multielectrode array suggesting that this neurointerface would not interfere with the target reinnervation and functional recovery. Behavioral studies showed partial motor function recovery in acute injured animals, demonstrating the ability of the interfaced peripheral nerves to reconnect with their original target organs.

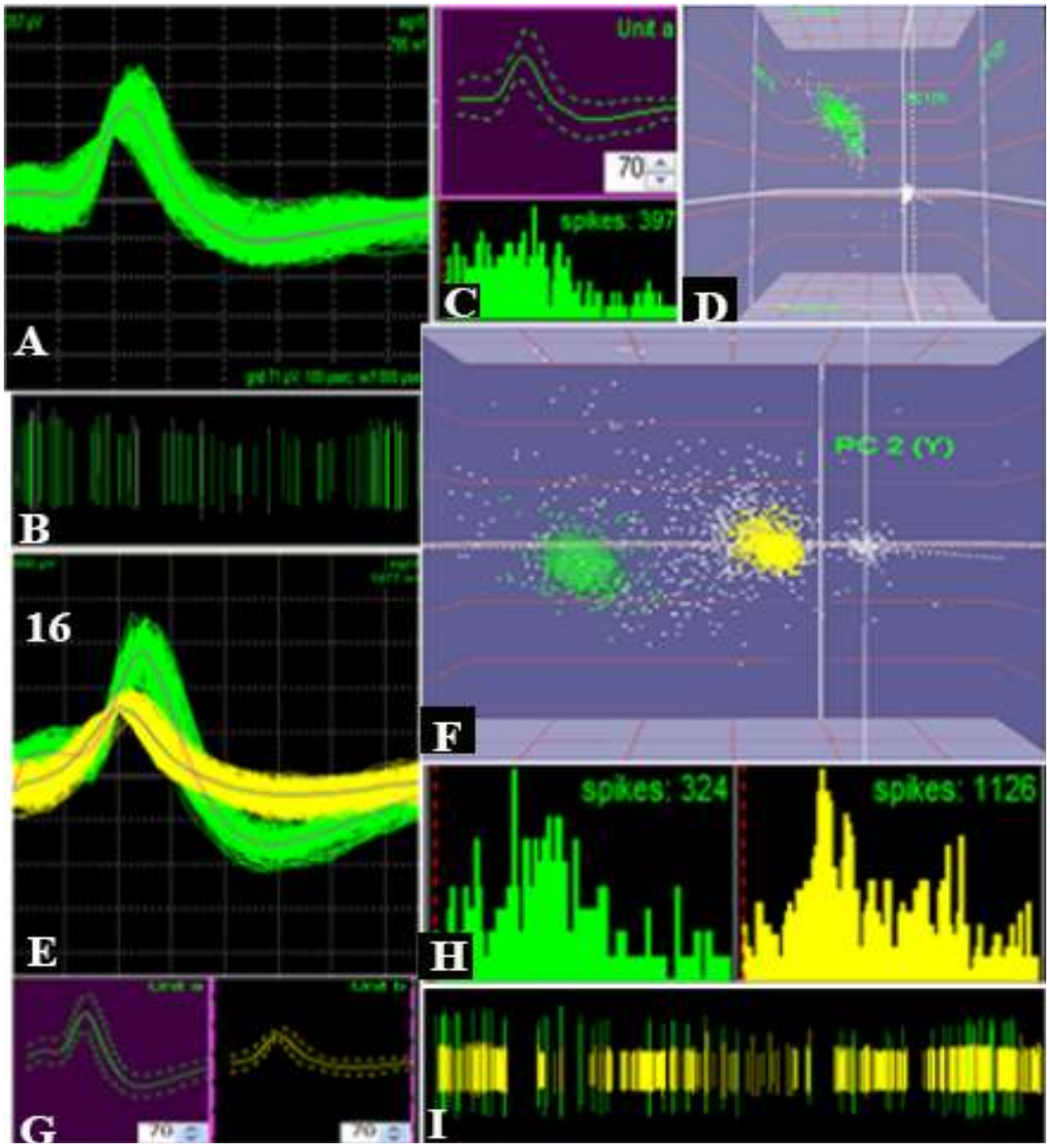

Figure 2.10: Single and multi-unit neural activity recorded in after neurointerfacing of a chronically injured nerve: A-D shows single unit firing whereas E-I shows multiple neuron activity recorded from a nerve with 203 days injury, demonstrating discrete neuronal activity after 8 days of regeneration. C,G shows waveform variability with limits marked by dotted line and mean with the solid line. Interspike interval histogram is shown in C and H for each of the units. D&F shows 3-D PCA plot with each cluster representing two discrete unit activities recorded from same electrode. B&I represent raster plots for each unit indicated by respective color. Time scale=100µsec in A, E and 40 min in B&I.

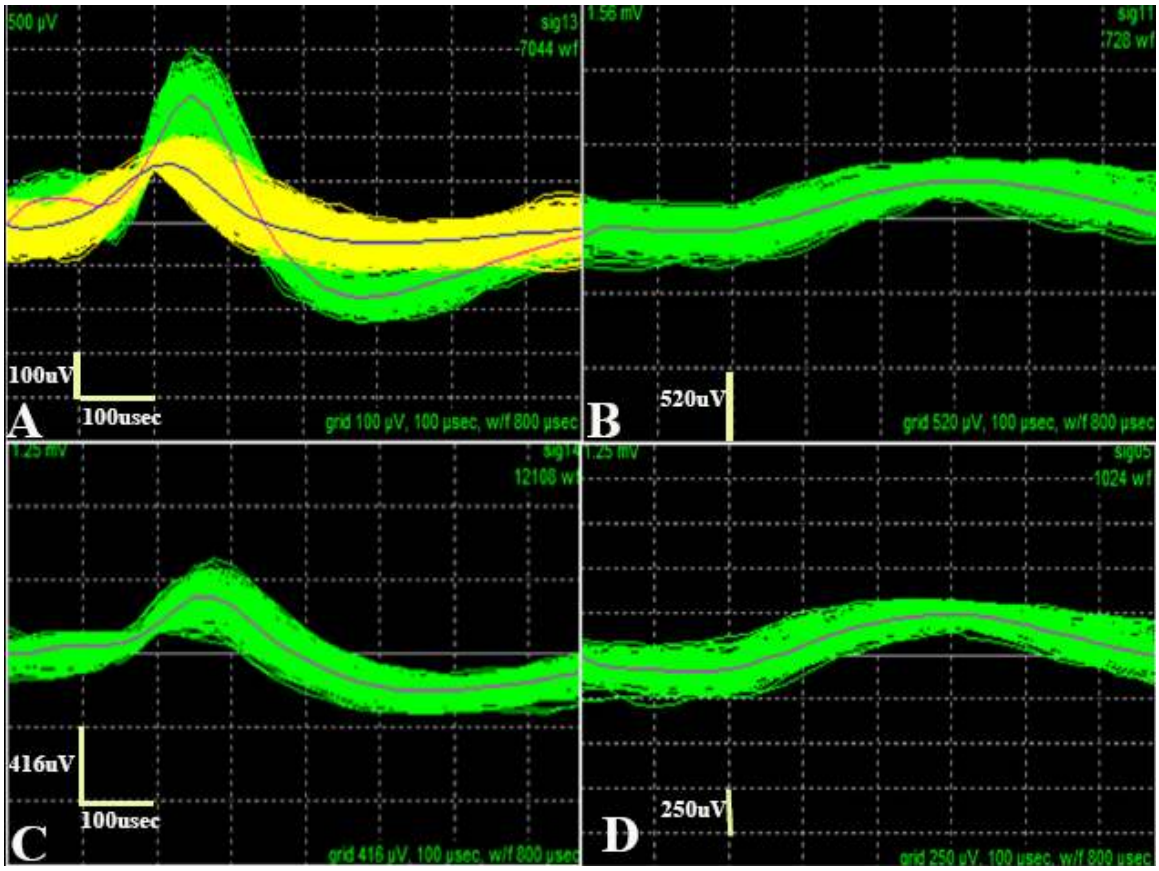

Figure 2.11: Time-related changes in neural activity from chronically amputated nerves. Neural activity from regenerating axons was recorded every week from implanted animals to observe changes in their firing pattern at different time points. Multi-unit and single unit activity recorded from a chronic injured nerve demonstrates discrete neuronal activity after 8 days (A,C) and 46 days (B,D) post implantation from same electrodes. Variability in the amplitude of recording is observed and one of the units was lost over time. X-axis scale=100µsec.

All animals from the chronic group exhibited complete paralysis of the injured limb throughout the experimental period whereas acute group animals showed better movements. Toe spread assay (n=2) measures the ability of an animal to stretch its toes as an indication of motor function recovery. As it can be seen from Fig 2.12D, toe spread index calculated as a ratio of extent of spread in injured to non-injured leg is approximately one in case of non-injured animals (acute positive control) indicating

unaffected motor control. Corresponding pictures (Figure 2.12A-C) above the bar graph shows the toe spread in correlation with the value of that particular experimental group. Whereas in case of chronically injured animals with no repair strategy where regeneration was prevented to their original target (transected and connected to an aberrant muscle; i.e., bicep femoris), ratio reduced to 0.4 and complete clawing was observed (Fig 2.12B). Animals with electrode implantation after acute injury with connection to their original target (end-to-end implant with nerve connected to the gastrocnemious muscle) showed improved toe spreading (TSI=0.75), indicating partial motor function recovery with statistical significance of $p \leq 0.01$.

Other physical and behavioral measures include hind limb motion and licking response. All animals which had undergone repair surgery showed limited motion of the injured hind limb compared to the contra-lateral control. Chronic group showed increased knee-joint flexion contracture as compared to acute due to muscle paralysis and non-usage. Following table shows the presence of licking response during the plantar heat where (√) represents positive response and X represents negative response. This gives an indication that there is sensory fiber regeneration leading to nociceptive recovery. Positive response of noxious pain along with the recovery in thermal sensation was seen only in acute but not in chronic injury group.

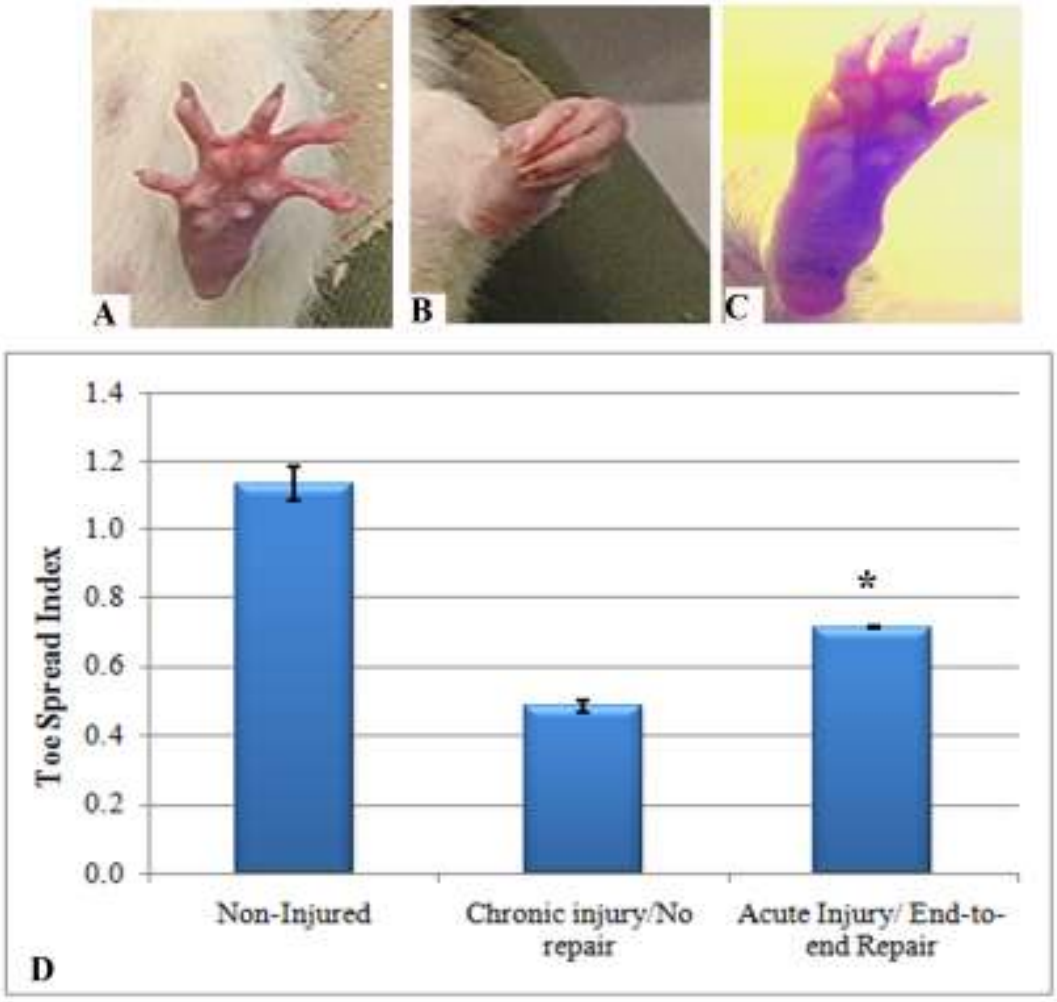

Figure 2.12: Motor function recovery after acute and chronic sciatic nerve transection. The toe spread index (TSI) was evaluated to determine functional reinnervation that occured despite neural interfacing to the multielectrode nerve guide. A-C is a representative picture showing paw of non-injured animal (A), chronically injured animals in which the nerve was attached to an abnormal target and acute injury group (C). D shows a plot of toe spread index against animal groups. Ratio is close to 1 in in normal non-injured animal but in case of chronically injured animal ratio dropped down to <0.5 which acts as a negative control. When end-to-end repair was done in acute injury model, index was ~0.75 indicating partial recovery of motor functions, Animals with acute end-to-end neurointerfacing allowed functional reconnection of regenerated nerves to their original targets. * indicates $p<0.05$.

Table 2.3: Assessment of licking response and nociceptive recovery

Animals	Licking Response		Latencies in injured animal
	Nomral leg	Injured leg	
Acute control	√	√	Normal
Chronic control	√	X	None
Acute repair	√	√	Intermediate
Chronic repair	√	X	Intermediate

Normal= 8-11 sec

Intermediate= 11-15 sec

None= >15 sec

Quantitative assessment of nociceptive (pain sensation) recovery was also done using plantar heat equipment and anesthesiometer, Ugo Basil, Italy. Paw withdrawal latencies (PWL) were measured in response to heat/prick stimulus in both the non-injured leg and the contralateral experimental side with their individual controls (n=2). The results of both these studies were highly variable and had inconclusive interpretations. This was due to the presence of chronic deformities like clawing, interphalangeal joint contractures and passive lifting of paws along the von-froy needle in case of animals with chronic injury.

2.3.8 Morphological analysis of Gastrocnemius muscle

Further validation of target reinnervation was done by labeling acetylcholine receptors at neuromuscular junction of the reinnervated muscle. The gross atrophy of the gastrocnemius muscle was observed on operated side in all the animals. There was 75% shrinking in myofiber area of acute injury group (2.14C-D) when compared to its contralateral control, whereas 91% shrinking was observed in the chronic injury group.

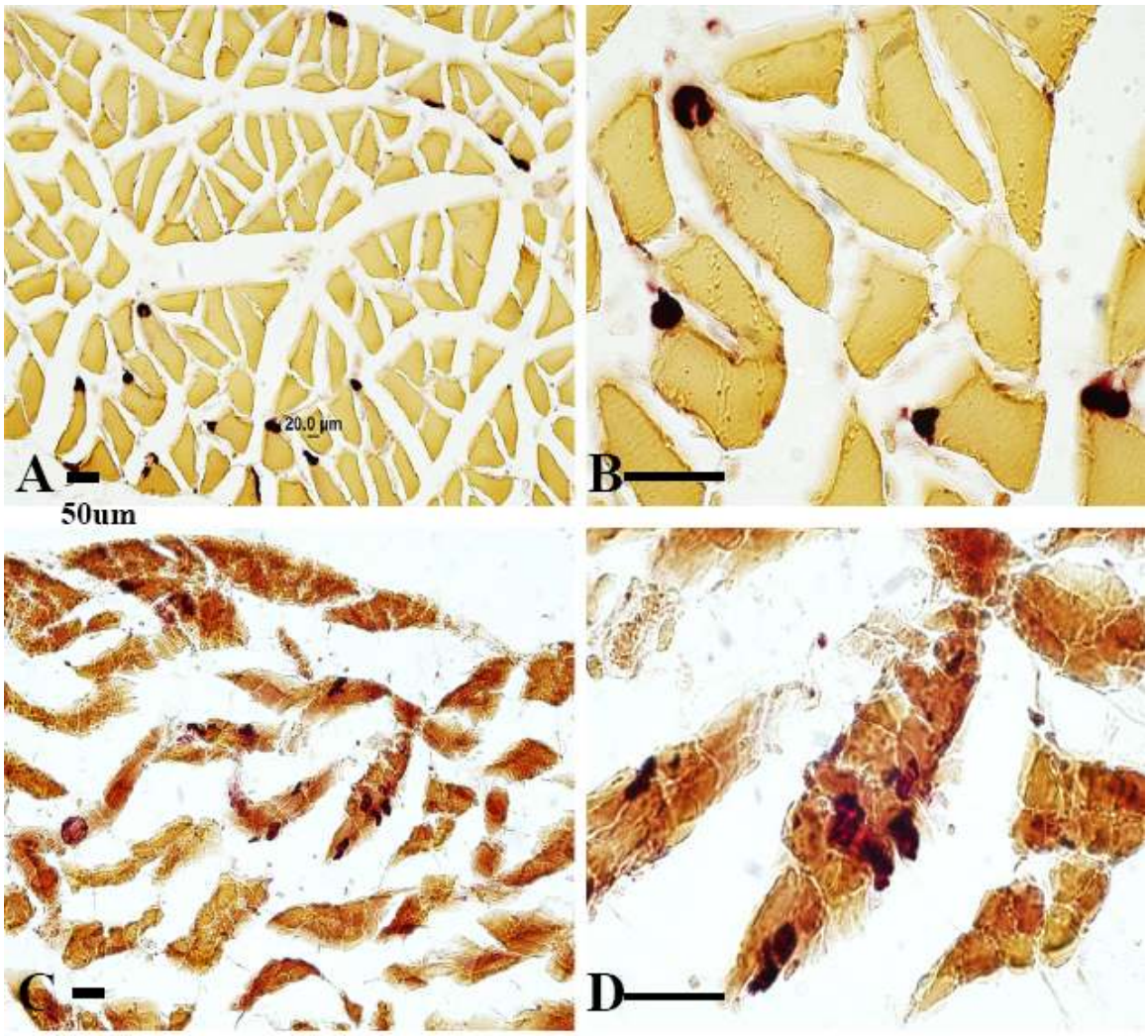

Figure 2.13: Muscle reinnervation in acute injury group: Light micrographs of cross-sections for acetylcholinesterase receptors (dark brown) present on neuromuscular junction (NMJ) of gastrocnemius muscle of non-injured leg (A&B) and injured leg after end-to-end repair (C&D) in case of acute injury animal with the survival of 49 days. The muscle fiber area in reinnervated muscle seems to be reduced as compared to that of normal. Scale bar = 20 µm.

In acute injury group, re-innervated muscle weighed 42% of the normal contralateral limb muscle whereas in chronic injury group, the atrophied muscle weighed only 13.6% of the contralateral control (n=2).

2.4 Discussion

Clinical trial have shown successful motor control of robotic prosthesis via brain-machine interface (Donoghue 2006) and myoelectrical signals from transferred nerves, which is challenged due to unstable neural interface. The novel regenerative interface where spontaneous nerve regeneration was facilitated through multielectrode arrays was developed to provide the long term stability of the implantable electrodes in peripheral nerves. In vivo functional assessment and thorough analysis of tissue interactions around the implanted electrode demonstrated robust axonal regeneration, limited inflammation and regeneration of both myelinated/non-myelinated axons. Two important milestones have been achieved in this study to develop a stable neurointerface. Placement of microelectrode array in a regenerative approach did not obstruct the regenerating axons facilitating functional recovery in acute injury group. Also long-lasting electrical recordings were obtained from both acute and chronically lesioned nerve further validated by positive histological results. This model successfully tested the ability of chronically injured nerve to form an interface with the recording device and proved that neurointerfacing chronically amputated nerves (5-6 months after injury) was as successful as interfacing the acute injured animals.

Result suggests that nerve regeneration and the overall healing process around the electrode array formed a more stable monolithic structure which appears less susceptible to use-related damage due to tethering forces and mechanical micromotion. These characteristics would predict a more stable interface for long-term use. The fact that this approach does not cause hindrance to the regenerating axons and facilitate them to

reinnervate the target muscle; it could be practically used for functional electrical stimulation for pain management, bladder control restoration and paralysis treatment.

2.4.1 Comparison of inflammatory response

Any foreign material in biological microenvironment induces immunological and pathological reactions which have detrimental effects on implanted electrodes and biosensors. Another cause of inflammation could be constant secondary injuries due to micromotions. Floating microelectrode arrays engineered to reduce tethering forces were used instead of conventional microwire-bundles which may have lead to minimization of secondary micromotions and thus limiting the inflammatory response. It has been shown that increased inflammation was observed around the implants which are tethered to the skull as compared to ones floating in brain tissue (Biran et al. 2007). Extent of inflammation is less in animals with short period of survival (<1 month) than ones with longer survival period (3-4 months). This observation correlates with the finding that macrophage accumulation near the foreign implant peaks after 2 weeks of implantation and then gradually decreases (Leung et al. 2008). In this study, reduction of activated macrophages surrounding the electrode could be also due to completion of nerve regeneration.

Invasion of macrophages in our study could most likely due to post-regeneration clearance of debris and foreign body host reactions, but not due to use-related injuries. It is important to study the extent of inflammation and develop techniques to minimize it since it directly affects the presence of axons in the vicinity of electrodes. Our results show that reduction in NFP+ axons was strikingly evident near in areas with intense

inflammation. It is important that axons are in close vicinity to the recording site since higher SNR can be achieved. This could further facilitate recording of low amplitude signals from the specific axonal types, thus affecting performance efficiency of the implant.

Table 2.4: Comparison of Regenerative and penetrating Interfaces

No	Regenerative Interface	Penetrating Electrode Interface
1	Natural regeneration of transected nerve, thus no tissue trauma	Insertion of sharp electrodes in intact nerve, thus causes tissue damage
2	Reduced inflammatory response and fibrous/scar tissue formation around the electrode surface	Electrodes gets separated from neuronal tissue due inflammation and fibrous/scar tissue formation
3	Closer contact of axons as they grow between the electrode pins (<50 μm)	Axons are relatively away from electrode pins (50-300 μm)
4	Reduced micromotion related injury due to better tissue-electrode integration	Micromotion of electrode pins causes secondary injuries to the surrrounding axons
5	Neural activity is unstable initially but number of units increase over time and eventually stabilizes.	Highest numbers of units are acquired in the start but recedes eventually.

2.4.2 Regeneration in acute and chronically lesioned sciatic nerve

Since regenerating axons regrow within the electrodes, better tissue-implant integration was obtained as opposed to penetration of electrodes in the intact nerve. Distribution of the electrodes along the nerve regenerative path in a non-obstructive way, allowed the growth of such neurons in proximity to the electrodes and the monolithic encapsulation of the array seem to have minimized the tethering forces and mechanical damage, normally associated to all the indwelling electrodes This would lead to stable

electrode-axon spatial configuration thus resulting into extended recording from same set of neurons. The regeneration rate in rat nerve falls within the range of 2-3.5 mm/day after nerve transection (Lundborg 2004). Complete regeneration was observed in the animal with 19 days of survival which determines that regeneration in both the experimental groups did not seem to be affected or delayed due to presence of electrodes which can tend to disrupt the gradient of cytokines formed by distal targets.

The number of active electrodes increased over time, reaching stability in number within the first 3 weeks, correlating well with the time needed for axonal regeneration through the nerve guide. Increment rate of active electrodes with respect to time is faster in acute group as opposed to chronic group which could mean that regeneration rate was slower in chronic injury animals than acute injury animals. Initial increase in number of active electrodes with respect to time could be because of axonal sprouting and electrodes coming in contact with regenerating axons but then the number stabilizes once regeneration is complete. Then process of tissue remodeling and reorganization takes place which changes the pattern of firing but not number of units. In acute injury animals, degenerating axons and the distal target secretes growth factors to attract the regenerating axons. However in chronically injured animals, reduced regenerative capacity could be associated with degeneration of distal Schwann cells, chronic axotomy and formation of neuroma distal to first nerve injury and absence of target specific molecules (Gordon et al. 2003; Jerregard et al. 2001).

Myelinated axons didn't seem to be compressed or degenerated in this study since space availability was not limited. On other side, sieve electrode has a closed design

which leads to thinner myelin sheaths (Ceballos et al. 2002; Lago et al. 2005) and compressive axonopathy (Lago and Navarro 2007; Lago et al. 2007a) at the interface. Numerous axonal sprouts from the proximal nerve stump tend to pass through via holes but undergo compression leading to axonopathy and distal degeneration as they start maturing. In this case, hampering of natural myelination process which is the support system for axons could affect the efficiency of the interface in long run. Limited space availability in the sieve electrodes leads to reduction in regeneration of highly myelinated, large diameter motor axons as compared to unmyelinated sensory axons. Motor axons did not tend to populate the entire area of regenerated tissue and were mostly found near periphery (Lago et al. 2005; Lago et al. 2007a; Negredo et al. 2004). Another possibility is that number of CGRP+ small and medium sized neurons in L4 DRG increase as compared to large diameter neurons after chronic injury. Thus better regeneration could be achieved by providing larger area with the compensation of the selectivity of recording from small number of axons.

2.4.3 Electrophysiological studies

It has been proven that current threshold for extracellular stimulation of the neurons increases with increasing distance between the electrode and the axon given by relationship, $I_{th}=IR+k.r^2$ where r specifies the distance between axons and recording site (Stoney et al. 1968). Also amplitude of the recorded signal in monopolar source varies inversely with distance in between electrode and source (Reichert 2008). Thus, it is imperative to maintain the close presence of axons near the electrode and avert all the factors involved in distancing or degeneration of these axons which imparts limited

functionality to the implant. Ideally limited inflammation and presence of nodes of ranvier closer to electrode surface would facilitate larger amplitude recordings, thus increasing the SNR. Theoretically, neural activity can be detected only from nodes of ranvier but not from those which are surrounded by insulating layer of myelin sheath (Mensinger et al. 2000). There is an increased probability of active site being near the nodes of ranvier in regenerative interface since the internodal distance in regenerated axons is highly foreshortened [240 µm-controls vs. 100 µm at 10 week post-transection, (Mensinger and Highstein 1999)]. Studies have not been done to determine minimum distance required for nodes of ranvier to be near the recording site to enable recording whereas in central nervous system, neuron firing within 100µm from the electrode surface results into spiking activity and further apart facilitates recording of local field potentials (Shoham and Nagarajan).

In our studies, nodes of Ranvier were found closer to the recording site whereas in sieve electrodes, nodes of ranvier are pushed away (Shimatani et al. 2003). In this study, variability in neural activity was noticed which could be caused due to constant neurochemical changes, alterations of excitatory and inhibitory connections, degeneration of distal nerve and sprouting of proximal ends and reorganization of somatosensory and motor maps. Single units on the electrodes were lost and the spiking activity was reduced on few of the electrodes which could be the result of increased inflammation or scar tissue formation around those electrodes. It has been reported that remodeled tissue has high tissue tortuosity (λ), given by $\lambda = (D/D^{*})^{1/2}$,where D is diffusion coefficient in water, D* that in obstructed medium ((Roitbak and Sykova 1999; Sykova et al. 1999).

This results into reduction in ionic permeability thus enabling electronic measurements only due to slow fluctuations in ionic concentrations i.e. low frequency firing. Reduction in neural activity could be also due to presence of cytokines and local fluctuations in extracellular concentration of potassium and calcium ions. Fibrous encapsulation or extensive inflammation around the electrodes increases the complex impedance of the electrode resulting into deterioration of the quality of spiking activity (Williams et al. 2007). We showed the ability of this novel experimental paradigm to record neural activity with an ability to distinguish single and multiple units. Our histological evidences show that open architecture leads to good regeneration of axons; however the selectivity to record from small number of axons is compensated.

2.4.4 Functional Recovery

Functional recovery was observed in animals that received an end-to-end implantation surgery where distal nerve was connected distally to their appropriate target muscle in which ability of acutely injured axons to regrow through the electrode array was tested. Regenerated axons were not only found to be in close vicinity to the electrodes, but were also able to reconnect to their target organ. In this group, motor and sensory function recovery was expected. However in case of chronically amputated nerves with 5-6 months of injury and absence of normal target which resemble the clinical situation of the upper extremity amputations, functional recovery was not expected.

We were not able to correlate any of the animal behavior to electrophysiological data because of the difficulty to train the subjects. This experimental design did not allow

any real-time implementations of computational models that can predict the animal's perceptual, motor, or sensory information from the residual nerves at the stump and allow this control data to neurally control the functioning of the robotic arm.

CHAPTER 3

NEUROTROPHIN INDUCED SEGREGATION OF DIFFERENT SUBSETS OF SENSORY NEURONS

3.1 Background

Years of research in neurobiology has exposed number of factors which aid in axonal guidance and regeneration in the transected adult nerve. These include cell adhesion molecules (L1, NCAM, N-cadherin) (Smith and Romero 1999; Thanos et al. 1998), molecules for axon guidance and path-finding (Semaphorins, Slits, Netrins, Ephrins) (Dickson 2002), and synaptogenic factors (Agrin, S-laminin, and ARIA) (Ruegg 1996). Levi-Montalcini studies has proved that neurotrophins and other growth factors secreted by target organs play critical role during the process of development when excessive death of sensory neurons was observed subsequent to removal of distal target. The cells lined along the pathway and target organs secrete neurotrophins which play critical role in supporting survival and differentiation of processes of the different subsets of neurons.

3.1.1 Neurotrophins

The neurotrophin family includes nerve growth factor (NGF), brain derived neurotrophic factor (BDNF), NT-3, NT-4/5, glial-cell derived neurotrophic factor (GDNF) mediate their effect by binding to high affinity receptor tyrosine kinases of the trk family (trkA, trkB and trkC) which have greater ligand selectivity or low affinity p75 receptor, a single transmembrane glycoprotein that binds to most of the neurotrophins.

These neurotrophins once attached to the receptor are internalized and retrogradely transported to soma of the neuron where intracellular signaling cascades are activated (Terenghi 1999). NGF preferentially binds to trkA receptors present on sympathetic neurons, sensory neurons of the dorsal root ganglion (DRG), BDNF and NT-4 to trkB and NT-3 to trkC but also can interact with trkA and trkB with low affinity (Jelsma and Aguayo 1994). TrkC receptors are present on large spinal sensory neurons, motor neurons and the noradrenergic neurons of the locus coeruleus. Among sensory neurons in dorsal root ganglion, expression of mRNA encoding trkA, trkB, trkC or p75 is restricted to certain sub-population representing approximately 41%, 33%, 43% and 79% of DRG neurons, respectively (Karchewski et al. 1999). All the neurotrophic factors have chemotactic effect that can influence extension and orientation of growing neurites.

NGF was the first neurotrophic factor isolated and identified by assaying sensory neurons and sensory ganglia. NGF is a dimeric 26-kDa neurotrophic factor that plays an important role in survival of sensory neurons and outgrowth of regenerating sensory axons after nerve injury. TrkA+ neurons are small diameter neurons with unmyelinated axons that mediate pain perception and express calcitonin gene-related peptide (CGRP). Also mRNA for NGF in nerves is usually found in low concentration but is dramatically up-regulated in the distal segment after the injury. It has no influence on motor neuron or their regenerating axons since they have trkB and trkC receptors.

NT-3 is a neurotrophic factor for trkC+ proprioceptive subset of sensory neurons that senses body position and innervates muscle spindles, golgi organs on the tendons. Mice with targeted mutations in either NT-3 or trkC receptor have shown severe losses in

proprioceptive neurons and slowly adapting mechanoceptors (Ernfors et al. 1994). NT-3 also plays critical role in promoting growth of motor neurons in vitro.

Semaphorins are a large family of secreted and transmembrane signaling proteins that regulate axonal guidance in the developing nervous system. There are close to 20 different semaphorins isolated till date. Sema3a, a typical secreted semaphorin is a potent inhibitor of axonal outgrowth from motor neurons in embryonic dorsal root ganglion. Its effect is mediated by its binding to distinct transmembrane receptor family of neuropilins (NP) but not plexin. However sema3a has high affinity for a complex formed by NPs and plex. Thus, plex proteins provide a signaling moiety in a receptor complex for the class 3 semaphorins, where NPs provide the ligand-binding sites. When sema3a binds to the receptors present on the neurons, rapidly induces actin depolymerization, growth cone collapse, augments antero- and retrograde axoplasmic transport resulting into inhibition of neurite outgrowth (Goshima et al. 2002). Sema3a provides motor axon with guidance cues by inducing collapse of growth cones of spinal motor neurons and repel motor axons in vitro (Cohen et al. 2005; Varela-Echavarria et al. 1997).

3.1.2 Experimental Design

Some studies have proven that the receptors which guide the extending axons during the development continue to be functional in adulthood; thus, it may be possible to exogenously provide essential neurotrophic factors to segregate or appropriately guide the regenerating axons from transected nerve. The receptors present on growth cone responds to the cues present in microenvironment by undergoing morphological changes and reorganizing the cytoskeletal proteins.

Different types of neurons have specific morphological traits. For instance, processes from trkA+ nociceptive neurons are long and unbranched whereas that from trkC+ proprioceptive neurons are highly branched and shorter in length. Axons can be efficiently guided by artificially introducing gradient of attractive and repulsive signals in the compartment. Segregation of mixed sensory fibers from dorsal root ganglion neurons was tested in 2D compartmentalized in vitro model made of PDMS containing desired neurotrophins in each chamber. Unlike the natural microenvironment laid by basal lamina which consists of attracting and repulsive molecules laid on the path of regeneration, synthetic material based regenerating conduit lack these specific cues which help neurons to decide their path.

Studies have also shown better regeneration of chronically injured nerves with neurotrophic support especially NT3 and NGF (Raivich and Kreutzberg 1987; Rich et al. 1987). In case of nerve gap repair where fascicular structure is no longer present, growth factors or other molecular cues could be synthetically provided for guided nerve regeneration. Similar attempt was made in the following study to sort regenerating axons to increase specificity of recording/stimulation in regenerative interface. Thus, this in vitro model was extended to the in vivo model where Y-shaped microrenathane conduit filled with appropriate trophic factors in each arm was used to preferentially segregate/enrich motor as well as sensory axons in regenerative context.

3.2 Methods

3.2.1 Dorsal root ganglion explants culture

The neonate (P0-P3) rat pup was anesthetized by inducing hypothermia using ice followed by decapitation. The spinal cord from thoracic level till the sacrum was extracted and cleaned on the ventral side. Lateral sides of the vertebrae column were trimmed closely to expose the spinal cord and DRGs attached to it. DRGs were freed from the bony fossa with the help of nerve cable exiting the spinal cord. The entire spinal cord attached to the DRGs by central processes was transferred to another petridish containing hank's buffered salt solution (Gibco; Carlsbad, CA). Tungsten wire was used to make a clean cut across peripheral and central nerve processes.

3.2.2 Two dimensional assay fabrication

Segregation of nociceptive and proprioceptive sensory axons was tested using 2D compartmentalized model made of polydimethylsiloxane (PDMS) elastomer which consists of a smaller diameter circular well where DRG was placed; two larger diameter wells to hold gelfoam soaked in neurotrophin containing media; and two channels connecting gelfoam containing well to the DRG containing well. Mixture of PDMS base and curing agent in ratio of 1:10 was heated up to 50^{o}C for 2 hours for polymerization and subsequently cooled. First generation molds were made by putting the mixture in negative mold consisting of "Y"-shaped feature placed on glass slide chamber as shown in 3.1A. To achieve finer edges, release agent was used on the negative mold which made the PDMS molds non-adherent to the glass slide. Thus, the method of fabrication was modified in which well was created in the polymerized PDMS sheet using biopsy punch

and scalpel was used to cut fine channels connecting them. These molds were autoclaved before use and then placed on the glass slide. After applying a thin coat of growth factor reduced extracellular matrix (ECM), assay was allowed to polymerize in 37^{o}C for 30 minutes. Then explants were carefully placed in the mid-lower portion of the PDMS

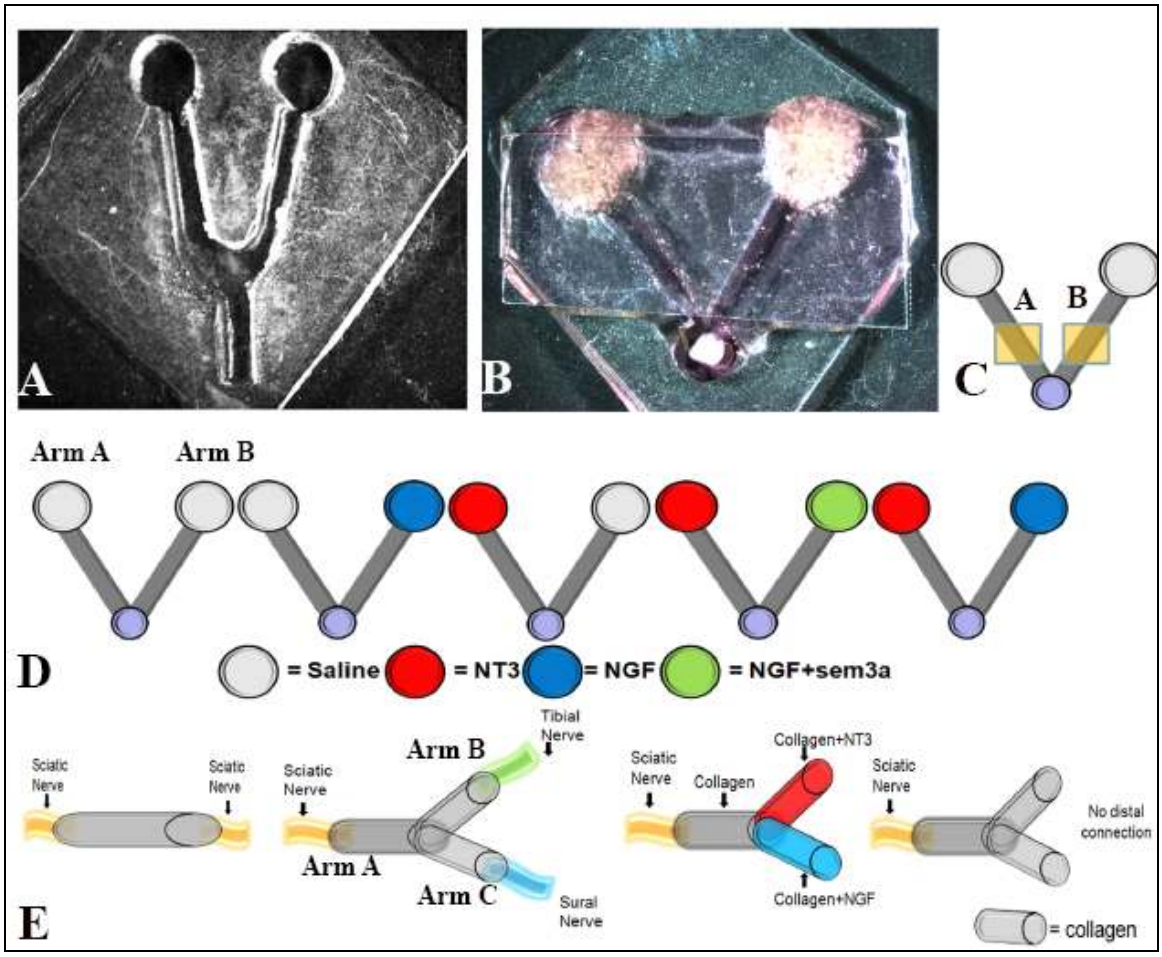

Figure 3.1 Schematic of PDMS assays and experimental groups for segregation: First (A) and second (B) generation of two dimensional PDMS assays for testing in vitro axonal segregation. B shows schematic of the experimental set-up where gelfoam soaked in appropriate solution is placed in two of the larger wells and DRG was placed in the center well. Coverslip is placed after adding media in the mold. C shows the region of interest where images were taken for quantification studies. D illustrates experimental groups for in vitro segregation where each treatment is indicated by distinct color. Similarly four experimental groups for in vivo segregation studies are shown in E.

mold as shown by in 3.1B and were embedded using drop of growth factor reduced ECM. After polymerization, neurobasal culture medium (Invitrogen, Carlsband, CA) supplemented with L-glutamine (Gibco Invitrogen, Carlsband, CA), B-27 supplement (Invitrogen, Carlsband, CA), and penicillin/streptomycin (Gibco Invitrogen, Carlsband, CA) was added.

The explants were then cultured for 2 days subsequent to which gelfoam pieces (3mm x 3mm) soaked in appropriate neurotrophin solution (mNGF, 10ng/ml,Sigma, St. Louis, MO; hNT-3, 25ng/ml, Sigma, St. Louis, MO; and sema3A, 40 ng/ml, R&D systems) were placed in the wells. Coverslip was placed on the mold to prevent floating of the gelfoam and cause delay in neurotrophin dilution in the media. Figure 3.1B shows the above explained experimental set-up used for testing in vitro segregation and the experimental groups are shown in 3.1D.

3.2.3 Gradient formation studies

Experiments were performed to ensure that two neurotrophins placed in different compartments do not spill over in the adjoining chamber and also form increasing gradient from the DRG containing well towards the neurotrophin source which is important for chemotactic guidance of axons. Two pieces of gelfoam loaded with Cy2 (897Da-green) and Cy3 (765Da-red) were placed in two compartments to determine amount of time required for two solutions to mix with each other in DRG containing well. Albumin of bovine serum (BSA) conjugated alexaflor-594 (66kDa) was used to test the gradient formation since its molecular weight lies between molecular weights of the neurotrophins (NGF=135 kDa, NT-3=27 kDa and sema3A=93 kDa) used in this study.

Digital tiled images covering the entire mold area were captured every 3 hours in case of gradient studies and every one hour in spill-over study using laser scanning microscope. Both the experiments were done until the time where gradient was lost and growth factors mixed in the other compartment. Profile function was used to obtain optical intensity spectra for the distance marked in the specified region of interest. Experimental conditions were maintained inside the imaging chamber during both the studies.

Table 3.1 Different groups for in vitro segregation using compartmentalized PDMS mold

Groups	**Treatments administered in each arm (Arm A/ Arm B)**
Group 1 (n = 3)	Saline (Control) / Saline (Control)
Group 2 (n = 3)	Saline (Control) / NGF
Group 3 (n = 3)	NT-3 / Saline (Control)
Group 4 (n = 5)	NT-3 / NGF + sema3A
Group 5 (n = 8)	NT-3 / NGF

3.2.4 Immunocytochemical analysis

Explants culture was fixed 2 days after the placement of gelfoams using 4% PFA. Cultures were washed 4 times with 1X PBS before immunocytochemistry studies. Refer 2.2.4 for general staining protocol. Briefly, DRG cultures were permeabilized in 0.25% triton-X for 30mins at room temperature and then blocked by 1% normal donkey serum in 0.25% triton-X for another 30mins at room temperature. Regenerated axons from the DRG explants were labeled with β-tubulin (mouse anti-b-tub, 1:500; Sigma, St. Louis, MO) which is a major building block of micro-tubules.

3.2.5 In vivo segregation

Three dimensional implantable "Y"-shaped conduit was designed using microrenathane tubing. The common arm in all the groups was filled with collagen and 3.1E shows the treatments in each of the arm for all the four experimental groups (n=8). Implantation was done near the bifurcation point of sciatic nerve where it divides into tibial, peroneal and sural nerve. After the completion of desired post-implantation period, all the animals were perfused with 1XPBS mixed with 1% heparin (to prevent blood clotting). 4% paraformaldehyde was flushed through the body followed by saline and the implant was harvested from left sciatic nerve. (Studies up to this point were done by Amit Chouhan. Refer 2.2.4 for detailed immunofluoresence staining method). Double labeling studies were done on longitudinally cut cryosections using N-52 which is a specific marker for all myelinated fibers which could consist of motor axons along with the proprioceptive fibers and CGRP, which specifically labels trkA+ sensory axons consisting of unmyelinated pain fibers.

Table 3.2 Different groups for in vivo segregation using Y-shaped conduit

Groups	Description	Arm B	Arm C
1 (n=8)	Straight tubing	NA	NA
2 (n=8)	Y-implant filled with collagen (positive control)	Tibial nerve	Sural nerve
3 (n=8)	Y-implant filled with neurotrophin+collagen	NGF + collagen No nerve connection	NT-3 + collagen No nerve connection
4 (n=8)	Y-implant filled with collagen (negative control)	No nerve connection	No nerve connection

3.2.6 Image analysis and quantification

For in vitro segregation studies, digital images of 20x magnifications were obtained using confocal microscope (Zeiss LSM 510 Meta). Number of branches for each axon in that field were counted to quantify mean number of branches per axon in all the experimental groups (n=3 to 8). All the branches per axon present in the digital image were traced and their lengths were measured to calculate mean branch length. Neurite processes longer that 20 μm were considered to be the axons.

For in vivo segregation studies, three stacked images of the A, B and C arms were captured using confocal microscope for each subject. Double-level standardized optical density threshold was applied to subtract the background and the saturated intensity values. A circle of fixed area ($0.03mm^2$) arbitrarily selected was placed over three randomly selected positively stained areas for fiber growth quantification. The area (in μm^2) of positively stained N52+ axons and CGRP+ axons, occupied by intensity values within the window of threshold values was measured individually in all three arms.

3.2.7 Statistical analysis

Entire dataset was expressed as mean± standard error. Data was analyzed using student-t test with unequal variances. A level of $p<0.05$ was considered to be statistical significant.

3.3 Results

The main objective of this study was to entice growth of specific sub-types of sensory axons in the channels containing appropriate neurotrophin combinations.

3.3.1 Gradient formation in response to passive diffusion from gelfoam

Studies to determine gradient formation were conducted using BSA-Alexaflur594. Fig 3.2A shows tiled image of the assay containing neurotrophin reservoir on the top and negative gradient formed along the length of the channel 3 hours subsequent to the addition of gelfoam. The intensity profiles increased over time in the channels due to continuous passive diffusion from the gelfoam. Intensity spectrum over the distance marked by black arrow in each of the channels is shown in Fig 3.2B&C. Lower intensities are seen near the origin of the line (start of the channel) which is farthest from the neurotrophin source and increase as it is traced towards the source indicating that gradient was formed. Gradient seemed to be lost six hours after the placement of gelfoams loaded with BSA-alexaflur-594.

Amount of time required for two solutions to mix in the DRG containing well was determined by using two colored dyes placed in the arms. 3.3A shows tiled image of the assays 4 hours (A) and 8 hours (B) after the addition of dyes. Diffusion of both the dyes in their respective arms can be seen. Intensity profiles for each of the dye (represented by their respective color) for the horizontal line drawn in the common region shows that two dyes were not mixed after 4 hours (C) indicated by opposite trends in two spectra i.e. green intensities decreases and red intensities increases from left to right. However both the spectra overlapped after 8 hours indicating that both the dyes mixed in the common well. It is important to study this, since dorsal root ganglion is placed in this region and also neurites sprouting initiates at this level. Qualitative images represented by different colors representing specific intensity range for the arm containing green dye (E) and that

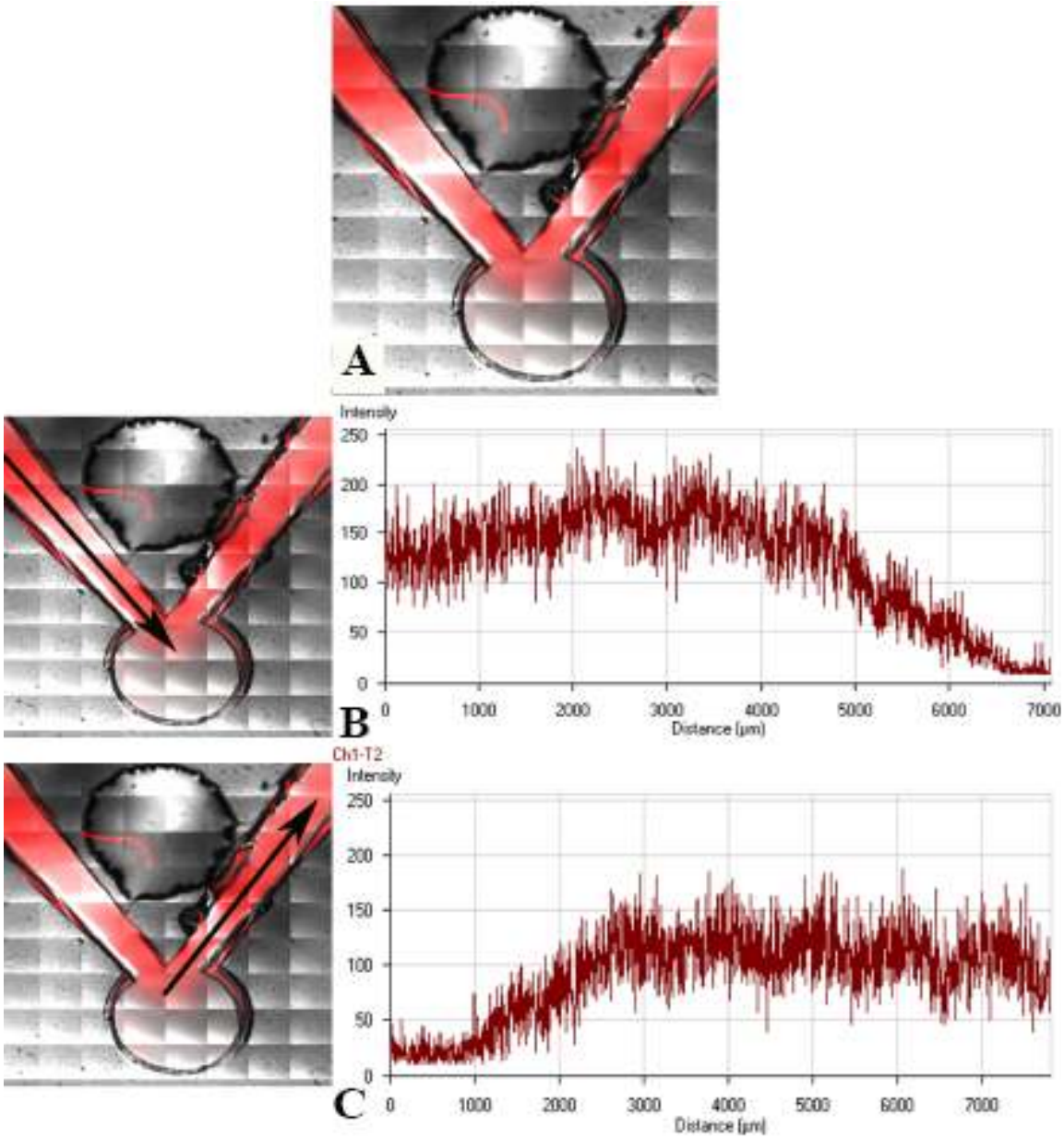

Figure 3.2 Gradient formation along the channels: A shows a tiled image where diffusion of BSA-594 from the soaked gelfoam placed in the top well is seen 3 hours subsequent to placement of gelfoam. B and C show the intensity profiles along the distance marked by the black arrows in the channels on the assay (Origin of the arrow marked the start of the intensity spectra). Decrement of intensities from neurotrophin source towards DRG (B) evidently indicates the formation and preservation of the gradient along the channel.

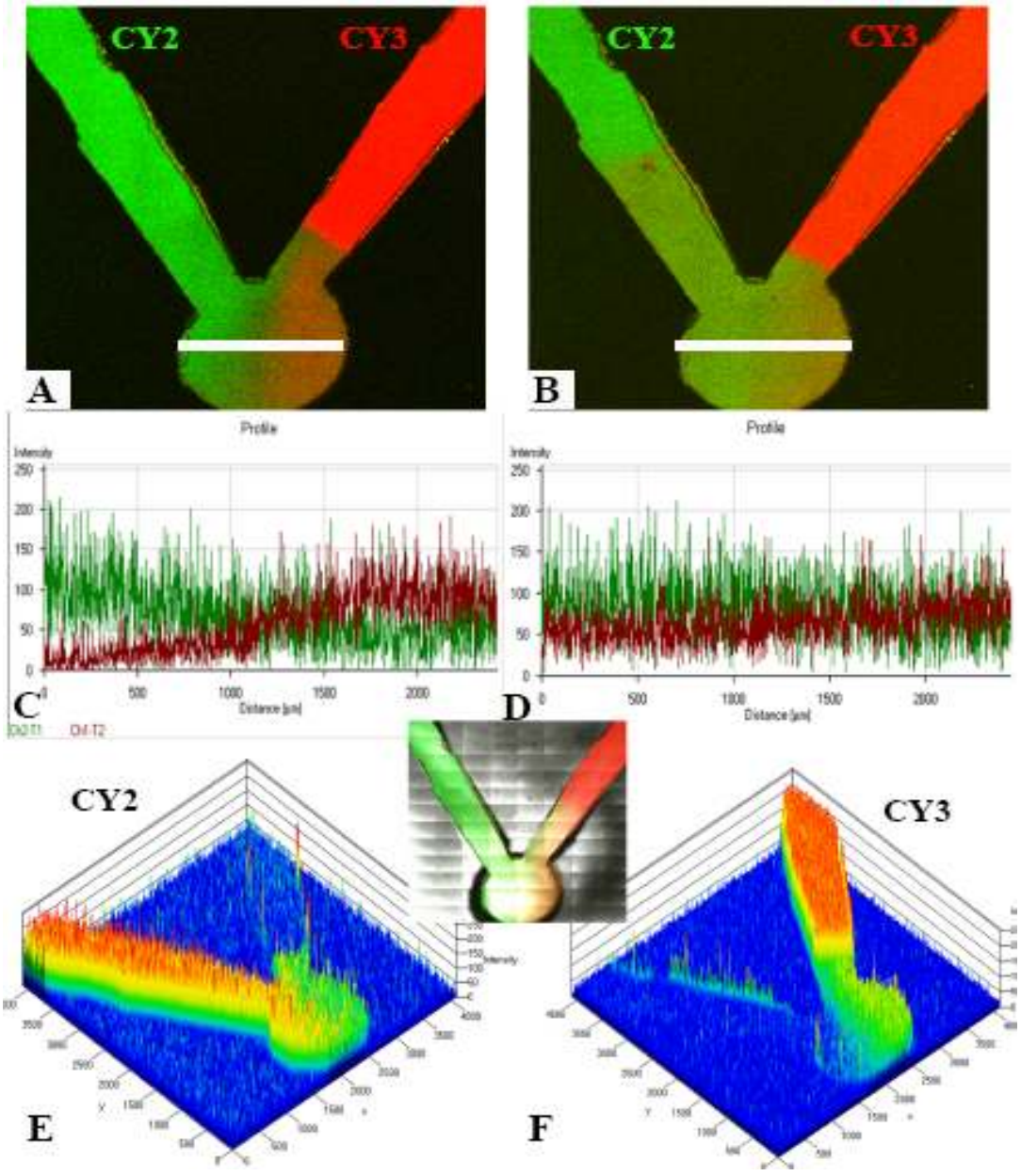

Figure 3.3 Gradient formation in the DRG containing well: A and B shows tiled confocal images showing diffusion of two different dyes CY2 (green) and CY3 (red) along their respective channels after 4 hours (A) and 8 hours (B). C and D show the intensity profile along the marked white line drawn where the DRG is placed in the center well. Opposite gradient trends i.e. red increasing from left to right and decreasing intensity of green dye along the same direction is seen after 4 hours which is lost after 8 hours indicated by straight profiles for both the dyes. Qualitative images shows gradient formation by green dye (E) and red dye (F) represented in different color shades along the length of the channel after 4 hours of gelfoam placement.

containing red dye (F). it could be seen in both the arms that red bars near the source of dye changes to yellow and then green as it reaches near the common well, thus confirming the presence of gradient.

3.3.2 Morphological evaluation of axonal outgrowth

Axonal growth from dorsal root ganglion was observed in all the assays of all the groups. Axons managed to reach halfway in the channels in response to negative gradient of the

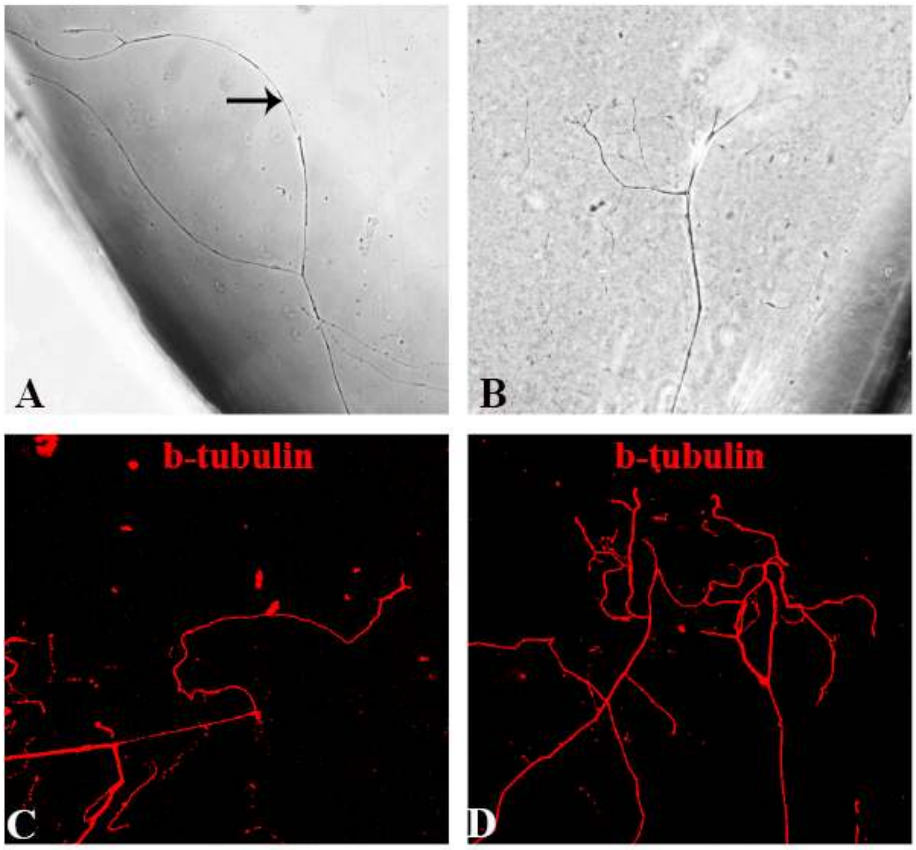

Figure 3.4 Morphological traits of nociceptive and proprioceptive fibers: Light micrograph of axonal outgrowth in NGF containing arm (A) and NT-3 containing arm (B) is shown. Distinct difference in their morphology can be noted where trkA+ noceptive pain fibers which are attracted by NGF are long and do not tend to be branched whereas trkC+ proprioceptive axons shows nodal branching (B) and interstitial branching (D) along with the shorter axonal lengths. C and D shows confocal image of the same.

neurotrophins. Figure 3.4 shows light micrograph (A) and immunocytochemical visualization (C) of the minimally branched long axons grown in NGF containing compartment. Similarly light micrograph (B) and confocal image (D) of axons in NT-3 containing chamber which display nodal branching in few cases and interstitial branching in most of them. Few samples from the later group showed formation of neurite tangles. Morphological assessment of axons in the control group was critical to clearly demarcate the morphological differences in nociceptive and proprioceptive fibers. Our results indicate that the axonal pathways of sensory neuronal subtypes can be altered by providing localized target derived cues along the routes of regenerating sensory axons.

3.3.3 Axonal growth assay in concentration gradient channels

Overall axonal outgrowth in assays containing neurotrophin was more than the control assay. For quantification studies, only those assays which had uniform and radial sprouting from DRG were selected to eliminate the chances of faulty estimation due to the preferential growth of axons in that channel. Figure 3.5 shows quantification of number of branches per axon for each of the groups where no significant difference in branch number was observed in both the arms of control as well as saline/NGF group. All the arms containing either saline or NGF in all the five groups contained approximately 1-3 branches per axon which matches with the normal morphology of the sprouted axons. However number of branches increases dramatically in all NT-3 containing arms of NT-3/saline, NT-3/NGF+sema3a and NT-3/NGF groups. The number of branches in NT-3 containing arm approximately doubled ranging from 4-7 branches per axon.

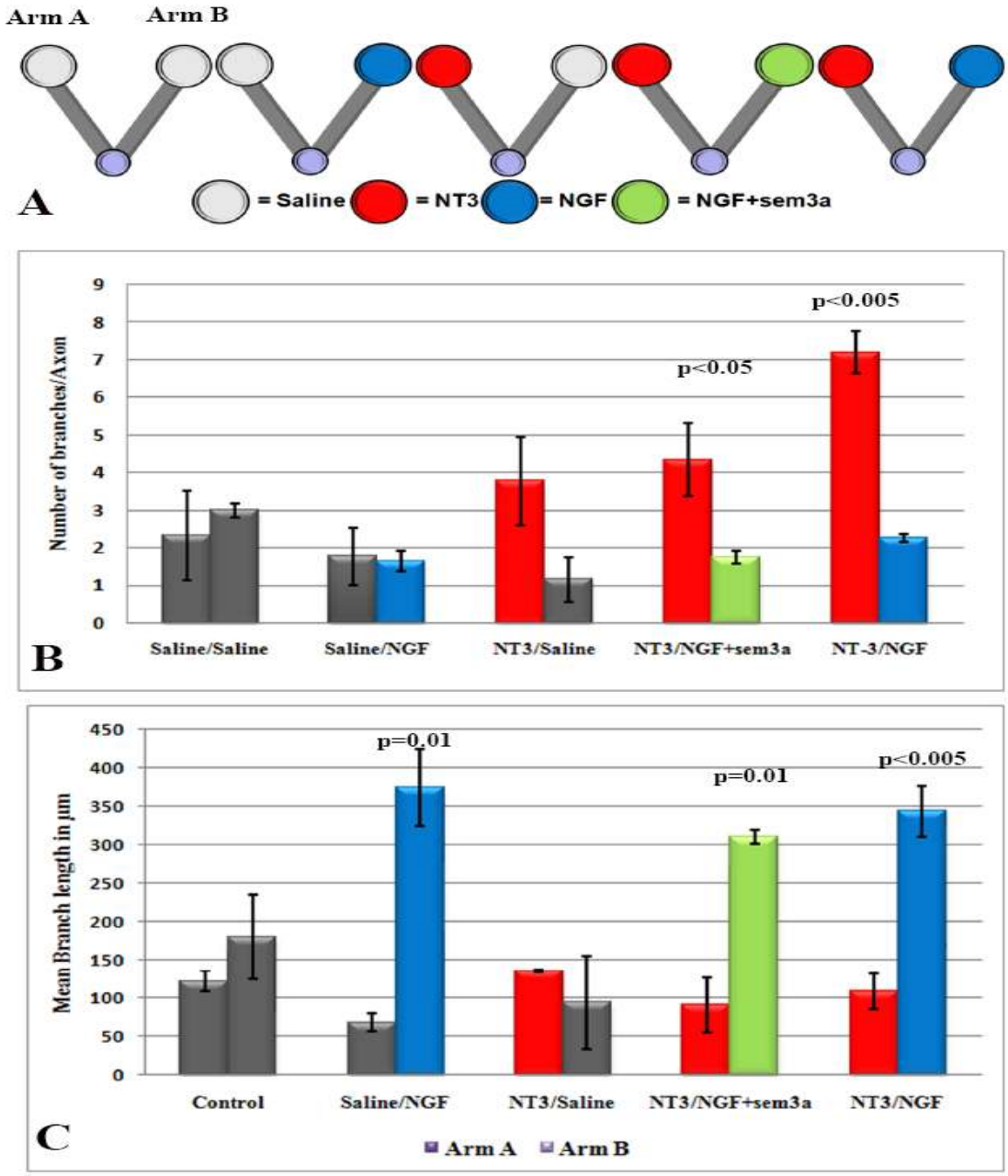

Figure 3.5: Quantification of axonal sub-types based on morphological traits: Schematic of experimental groups for in vitro segregation is shown in A. B shows quantification of number of branches per axon where significantly higher number of branches is observed in all NT-3 containing arms. Statistical significance was obtained in two of the NT-3 containing arms. Similarly mean branch length for each of the group is plotted in C. Presence of long branches was noted in arms with NGF soaked gelfoam. Statistical significance was obtained in all the groups.

Within the arms with NT-3 in all three groups, reduction in branch number was observed in NT-3/NGF+sema3A arm as compared to NT-3/NGF group indicating some involvement of sema3A from the adjacent arm. Mean branch number in NGF arm of NT-3/NGF group is slightly higher than that of NT-3/NGF+sem3a group suggesting that sema3a indeed enabled inhibition of proprioceptive fibers in that arm to some extent.

Quantification of branch lengths shows no evident difference in the arms of control group and in NT-3 containing arms of other groups. Approximately three fold increase in branch length of axons was observed in all NGF containing arms of saline/NGF, NT-3/NGF+sema+3A and NT-3/NGF group. Also average branch length in NGF+sema3A arm (green) of group 4 is slightly lesser than that of NT-3/NGF and saline/NGF group confirming the unknown interference of sema3A with branch lengthening. Statistical significance with p-value < 0.05 was achieved in three of the NGF containing groups.

3.3.4 Evaluation of in vivo sorting of regenerating axons from transected nerve

The ability of neurotrophins to segregate motor and sensory axons from regenerating sciatic nerve through "Y"-shaped implants was tested in this study. Two months post-operative, all the animals showed tissue growth in both the arms of the "Y" and were connected to the distal portion of the nerve. Immunofluorescence studies were performed on regenerated tissue double-labeled with N52 (A-C) to mark all myelinated axons and CGRP (D-F) which marks all nociceptive axons, subset of sensory axons. Figure 3.6 shows fluorescence image of regenerated tissue from positive control group where arm B (B,E) and C (C,F) are connected to tibial (motor) and sural (sensory)

respectively, where more axons labeled with N52 are observed in arm B as compared to arm C and contrarily increased amount of CGRP+ axons seem to be present in arm C. This observation indicates some positive role of target-secreted elements. Close observation of thickness/width of these stained axons indicates that myelinated axons (red) comprising of motor and proprioceptive axons in the arm distally connected to tibial nerve are thicker than the unmyelinated axons (green) present in the arm connected to sural nerve.

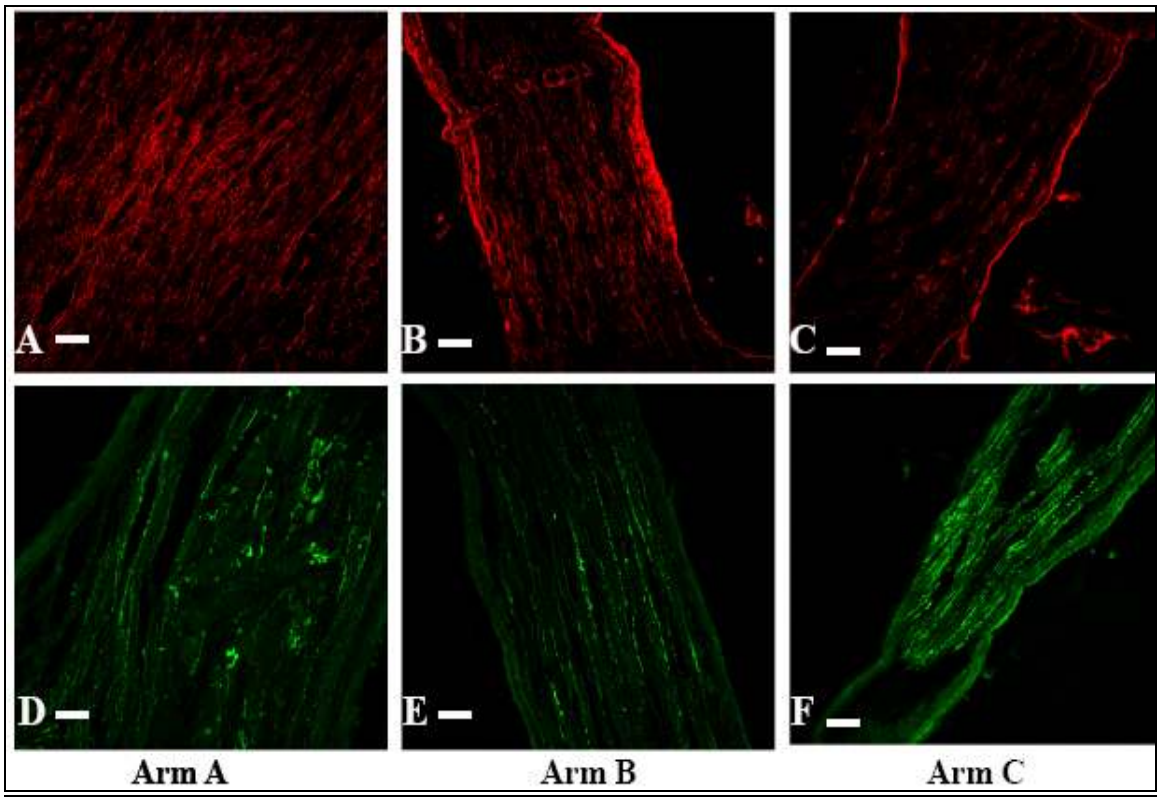

Figure 3.6 Preferential growth of myelinated and unmyelinated axons through the Y-conduit: N52+ axons (red) were found to be denser in arm B distally connected to tibial (motor) nerve as compared to arm C which is distally connected to sural (sensory) nerve. Similarly CGRP+ (green) unmyelinated fibers had regenerated in arm C. This suggests that there was enrichment but not segregation of certain sub-type of axons in the arms of Y-conduit.

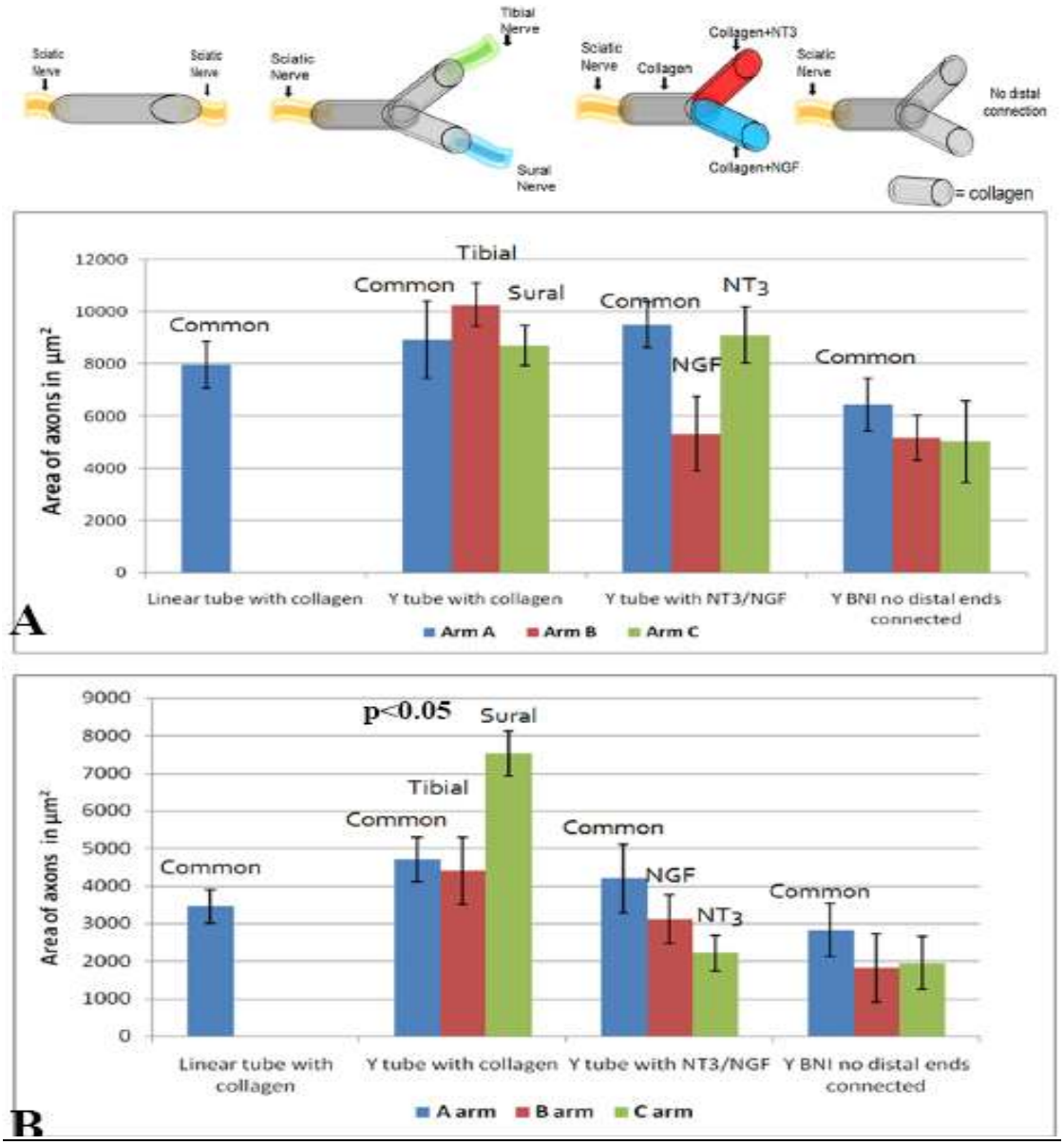

Figure 3.7: In vivo quantification of regenerated axonal sub-types: Schematic of four experimental groups for in vivo segregation studies are shown above. A shows the plot of N52+ axons for each of the group in all the arms. Mean axonal growth represented in form of area of myelinated fibers was found to be more in the branch distally connected to tibial and arm containing NT-3. Similar quantification of axonal profiles for CGRP+ fibers is shown in B. More unmyelinated axons were found to be regenerated in arm connected distally to sural nerve and arm containing NGF. Statistical significance was obtained only in positive control group.

The extent of sorting was evaluated by quantifying the axonal area of differently labeled fibers in all 3 regions consisting common arm (A), experimental B and C arm. Quantification of N52+ fibers shown in Figure 3.7 shows increased number of N52+ fibers in arm B of positive control group as compared to arm C connected to sensory nerve. In the experimental group, more N52+ fibers were found in NT-3 containing branch than the NGF branch. Similarly, quantification of CGRP+ fibers shows enhanced regeneration in arm C (connected to the sensory nerve) in positive control group with statistical significance ($p<0.05$). Mean axonal density of CGRP+ fibers in NGF containing branch is more than that of NT-3 containing arm in experimental group but is not statistically significant. Overall reduction in regeneration of N52+ as well as CGRP+ axons was observed in negative control group where there was no connection of conduit to the distal nerve. The fact that the axonal density profiles for N52+ and CGRP+ fibers in linear tube filled with collagen is similar to the values from all common arms suggests that bifurcation in the "Y" conduit did not hamper the axonal regeneration. An increased value for axonal area in the branches as compared to the common arm in positive control group indicates sprouting. These highly sprouted axons undergo the process of pruning in their later stage of regeneration.

3.4 Discussion

It could be observed that both the axonal types were present in both the arms to some extent leading to enrichment of particular sub-type of axons but not complete segregation within the compartment. All the axons were considered during the quantification of morphological traits leading to underestimation of extent of branching

or branch length in case of proprioceptive and nociceptive fibers respectively. Theoretically, addition of sema3a to NGF should have increased the mean branch length since sema3a blocks the growth of proprioceptive fibers. Observed results did not show any correlation with the theoretical. Also extent of branching was reduced in NT-3 arm of NT3/NGF+sem3a group indicating that sema3a could have mixed with media in the other chamber which had negative effect on branching of these axons. In this assay, morphological trait of nocicpetive fibers to have no branches or less number of branches was not evident when compared to the values of control group due to the randomness of axonal sprouting and non-optimized design of this assay. Similarly reduced branch length of arborized proprioceptive fibers was not noted as compared to mean branch lengths of control group.

Both trkA+ and trkC+ axons respond to NT-3 whereas only trkA positive axons respond to NGF. There is some extent of colocalization of the trk receptors on the growth cone of the regenerating axons. In recent studies, it was revealed that 10% of DRG neurons coexpress trkA and trkB mRNA; 19% coexpress trkA and trkC mRNA; and 18% coexpress trkB and trkC mRNA. Signaling via the trk receptors varies by select expression of the multiple isoforms of both full-length trkA and trkC receptors. There are two variants of trkA receptor, one without insert (trkA NO INS) and other with 6 amino acid insert. This region was found to have no effect on binding specificity and functional response but enhances the responsiveness of the receptor to NT-3. Also a full-length trkC spice variant reduces the neurite promoting capabilities of NT-3 (Karchewski et al. 1999).

Another question to be addressed here is whether particular sub-type of axons were guided to enter the channel with gradient of attracting neurotrophins or whether there was induction of elongation and arborization responses. This was difficult to know because axons were not stained for trkA and trkC specific antibodies. However, studies have proven that overexpression of NT-3 in rescued trkA+ neurons which undergo apoptosis during development, led to increase in number of proprioceptive neurons in L5 and 11-fold increase in soleus muscle spindles (Moqrich et al. 2004). This indicates that the branching effect in NT-3 containing arm could be observed in axons from trkC+ neurons or could be induced in axons from trkA+ neurons.

There was no element in this experimental paradigm to provide controlled growth factor delivery. Gelfoam, a hemostatic device was used since it is water insoluble, biocompatible and has capacity to absorb fluids 45 times its own weight. This property of gelfoam made them simple and appropriate candidate for usage as a growth factor reservoir. No significant difference in axonal growth of two sub-types of axons was observed in experimental groups. This could be the result for inefficient delivery system (dried collagen in this case) or inadequacy of neurotrophins used for sorting. There is a possibility that additional guidance molecules and growth factor combinations are required to sort regenerating axons from transected mixed modality sciatic nerve. There was no gradient formation in the in vivo animal experiments since neurotrophins were directly mixed with collagen.

Greater understanding of potent molecular and cellular cues presented by Schwann cells and their endoneurial extracellular matrix facilitates efficient guiding of

regenerating axons to their right targets (Dubovy 2004). Some researchers have focused on to study influential role of neurotrophins secreted by Schwann cells in segregating the axons (Fu and Gordon 1997). Few experiments evaluating the ability of various tissues to attract the regenerating axons have shown that nerve and muscle tissue have the most attracting power (Lundborg et al. 1986; Weis and Schroder 1989). Based on this concept, sorting of different sub-types of regenerating axons was attempted by using bifurcated conduit filled with target derived molecules in each arm to improve the functional recovery after peripheral nerve injuries (Jerregard et al. 2001). In this study, skin filtrate was used in a graft connected to sural nerve and muscle filtrate used to tibial nerve which consists mainly of motor fibers. Sorting of axons based on their function was achieved to some extent, thus supporting the idea that target derived molecules play a important role in attracting or supporting growth of certain sub-type of axons. Similar idea was used to segregate axons in vitro and in vivo using trophic factors to attain higher specificity of recording/stimulation for well-organized operation of prosthetic device.

CHAPTER 4

ENHANCEMENT OF ELECTROCHEMICAL PROPERTIES OF IMPLANTABLE ELECTRODES USING NANOMATERIALS

4.1 Background

Enhancement of the electrochemical stability of the metallic electrodes is of foremost importance to increase the longevity of the chronic implants in vivo. Thus these metal electrodes can be coated with materials which are more conductive in nature and yet chemically stable. Also surface modifications of the neural implants can be done to enhance the biocompatibility.

Various attempts have been made to improve characteristics of these electrodes by biological and chemical modification techniques. Biological modification includes neurotrophin incorporation, immobilization of cell adhesion molecules like laminin, dextran or peptides to attract neurons and entice them to sprout on electrodes before the inflammation cascade begins and other tissue engineering techniques to enhance the biocompatibility. It has been shown that adhesion of undesired cell types was reduced by modulating the topography of neural electrodes (Seymour and Kipke 2007). Chemical modification includes surface treatments or coatings are done to increase the effective surface area of electrode without compensating the geometrical dimensions of the exposed tip of electrode. Conventionally platinum black, pyrolytic carbon, iridium oxide or vitreous carbon coatings have been used commercially. But there are limitations to

these materials like Pt black are mechanically fragile and iridium oxide is chemically unstable.

Results from current literature has shown that carbon nanotubes (CNT) and conductive polymers (CP) like polyaniline (PANI), polypyrrole (PPY), poly(3,4-ethylenedioxy thiophene) (PEDOT) enhance the electrochemical properties of the neural implants like their impedance, capacitance and performance efficiency. Thus these conductive materials can be used as the suitable candidates. CNTs are inert, highly conductive, mechanically strong and biocompatible but lack high charge storage capacity like conductive polymers. CNTs have been proved to be better substrates for the growth of neurons and increase the efficacy of neural signal transmission. Unlike CNTs, CPs readily dissolve in water, so neurotrophic factors like NT3, NGF, BDNF, CNTF and others could be incorporated during the process of electropolymerization to suppress detrimental immune responses, promote neurite extension and attract different sub-types of axons. Studies have shown that electrical stimulation pulses could be used to achieve sustained and controlled neurotrophin release from conductive polymer network. Due to the complementary characteristics of CP and CNTs, composite materials could be used to coat the electrodes. CP-CNT composites have shown better mechanical integrity, higher electronic and ionic conductivity, larger electrode specific capacitance and greater stability. Carbon nanotubes can be applied mechanically by mixing with a binder which intrinsically has impedance or chemically to the metal surface. But there are limitations to these techniques like non-uniformity and non-specificity of the coatings on small exposed metal surface. Electrodeposition overcomes above mentioned limitations and has very

low contact resistance. Thus this technique does not interfere with impedance reduction due to the coating.

Specific aim of this project was to optimize the electrochemical performance of the commonly used implantable neural electrodes by using nanomaterials that will enhance the stability of tissue-sensor interface which will in return increase the longevity of the implantable device in vivo. We hypothesize that use of highly conductive and nanoscale materials would lower the impedance due to increase in the specific area which would increase sensitivity and SNR still retaining the dimensional selectivity. The bulk properties of these materials have high storage capacity which would further reduce the stimulation threshold and total pulse duration.

4.2 Methods

Aqueous solution of multiwalled carbon nanotubes (Cheap Tubes Inc, CA; 1mg/ml) manufactured by carbon vapor deposition (CVD) technique were mixed with 1/10th solution of potassium gold cyanide. pH was checked to ensure that the coating solution was acidic. Electrochemical Analyzer (CH Instruments, TX) was used to electrodeposit CNT-Gold composite on the electrodes using constant potential method. Controlled CNT-gold deposition was achieved using chronoamperometry technique in which amount of current passed in each step can be monitored over time.

All 18 electrodes from floating microelectrode array (FMA) were characterized before coating to get baseline values of impedance and charge storage capacity and again characterized after coating to note any change in the previously measured values. 11/18 showed electrical connection between electrode and head connector pin. Alternate

electrodes (6/11) were coated with CNT-gold composite so that the 5 electrodes become the control. Cyclic voltammetry (CV) is an electrochemical technique in which ramp potential sweep is bi-directionally applied between set limits to the electrode and the corresponding current values are measured between working and counter electrode is measured to study redox reactions at the electrode interface. In our study, CV was used to calculate charge storage capacity (capacitance) during pre/post characterization. Impedance spectroscopy (IS) is another technique which is used to characterize intrinsic electrical properties of any material and its interface by applying AC small amplitude voltage at variable frequencies. We used this technique to assess change in interfacial impedance pre/post coating and to study kind of interfaces formed by CNT with saline.

4.3 Results

Increase in the amount of current passed at each step was observed over time during the time of deposition indicating the decrease in electrode impedance due to coating of highly conductive material on the electrode. Total of 6 out of 11 electrically connected electrodes were coated with CNT-gold composite. Figure 4.1A shows the light micrograph of an array and subset showing higher magnification picture of the same. 4.1B shows SEM picture of the exposed tip of the metal electrode coated with CNT-gold composite. The impedances of all the electrodes ranged from 150K to 250KΩ at biological relevant frequency, 1 kHz before coating which drastically reduced to 8K-15KΩ after coating as indicated by impedance spectroscopy shown in 4.1C. Average reduction was 95% from the initial value. Higher reduction in impedance i.e. Z_i=10 MΩ to Z_f=1 MΩ, was observed to be near the lower frequencies where local field potential

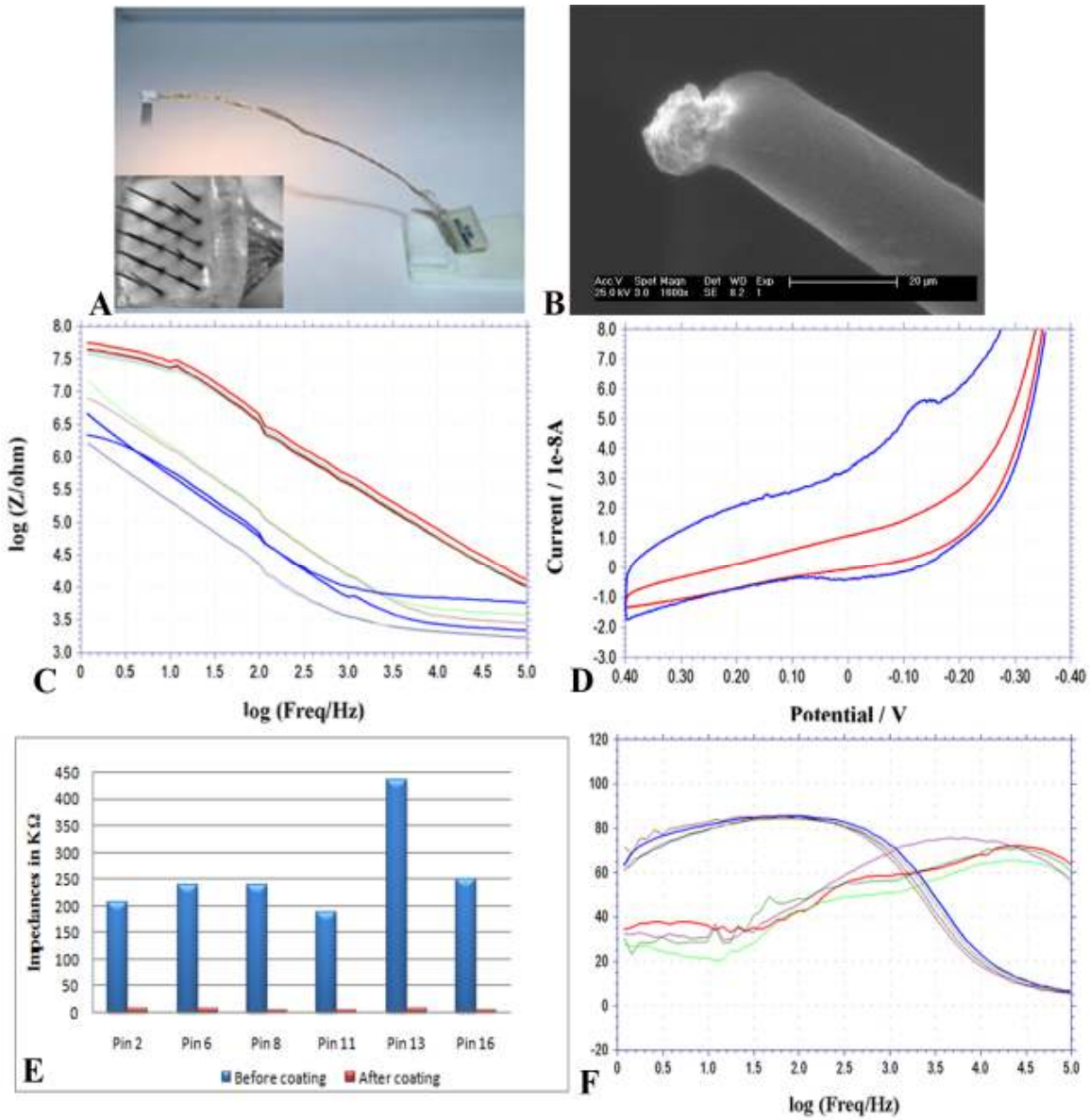

Figure 4.1 Enhancement of electrodes using nanotechnology: Light micrograph of floating microelectrode array is shown in A. B shows SEM picture of exposed tip of Pt/Ir single wire electrode coated with CNT. Qualitative images showing 100-fold reduction in impedance at biologically relevant 1kHz frequency of all six electrodes measured by impedance spectroscopy curves (C) and increase in capacitance calculated by cyclic voltammetry as shown in D. E shows the quantitative analysis of impedance change at 1KHz for coated and uncoated electrodes. Phase measurements for all electrode pre and post coating are shown in F.

occur. 4.1E is a plot showing change in impedances for each of the electrode where initial

impedances are represented by blue bars and reduced impedance post coating by red bars.

Final values were within quality control limits where variability was brought down from 200KΩ to 4KΩ by manipulating total time required for coating process based on initial impedance of the electrode. 4.1F shows phase angle measurements of each of those electrodes pre and post coating. Electrode-electrolyte interface becomes more capacitive than the uncoated electrodes at lower frequencies. It could also be observed that there is consistency in final impedance values and phase angle measurements though there were irregularities in initial values. 4.1D shows the cyclic voltammetry plot which was used to study the electrochemical characteristics of the coating material, and measure the charge storage capacity (capacitance) of the uncoated (red) and coated (blue) electrode. Oxidation peak is seen on the positive voltage scan of the coated electrode at -0.1V indicating large rise in current at that voltage. Specific capacitance increased from 3.5mF/cm^2 to 10.7mF/cm^2 i.e. 3.3 times the original value, which is not significant. Though we got drastic lowering of impedance after CNT-gold coatings, there was no significant change in its charge carrying capacity

To assess the physical stability of the coating material, changes in the relevant parameters were monitored over time. It was observed that impedance got doubled (5K to 10KΩ) when measurements were done after 24 hours of coating where electrodes were kept in air dried conditions (data not shown).

4.4 Discussion

Results show that CNTs were able to lower the impedance leading to enhancement of sensitivity without compensation of selectivity. This would in return facilitate recordings of low amplitude signals and enhance the SNR. Relationship

between noise and impedance is given by, $U_{th} = \sqrt{(4kTBR_{tot})}$ where k is the Boltzman constant, T is the temperature in degrees Kelvin, B is the frequency bandwidth and R_{tot} is the real part of the total electrode impedance (Gabay 2005). Theoretically, noise pick-up on coated electrode would be reduced since noise is directly proportional to the real part of complex impedance. The roughness of the CNT coated electrodes is expected to act as adhesion agents thus enhancing the cell-electrode coupling. Overall enhancement of quality of recording brings out small details and characteristics of the recorded waveform which further simplifies the separation of distinct units attributing to individual neurons. Evidences of biocompatibility of pristine CNT yarns is provided in Galvan et al, shown using increased proliferation and alignment of cortical neurons, cerebellum neurons and Schwann cells (Galvan-Garcia et al. 2007).

Carbon nanotube substrate has shown to increase the frequency of post synaptic currents measured using patch clamp method (Lovat et al. 2005). Carbon nanotube coating on the electrodes enhances the extracellular recording as illustrated in figure 4.2A. In a primary neuronal culture preparation, first and third quadrant represent signals recorded from set of electrodes coated with CNTs and uncoated ones respectively. 2^{nd} and 4^{th} quadrant shows signals recorded after stimulation pulse for the respective electrodes. More light blue dots were found in 1^{st} quadrant than 3^{rd} one indicating more signal energy was recorded in CNT coated electrode. After applying same stimulation pulse on both the sets of electrodes, augmentation of recording capability of CNT coated electrodes is evidently seen by presence of red and light blue dots in the 2^{nd} quadrant as compared to minimal change in 4^{th} quadrant (Keefer 2008). These results reveal that

voltage as well as current stimulation thresholds for CNT coated electrode are lower than metal electrodes; implying long term stability and functioning of the neural interface. This is possible because the modified electrodes have an ability to induce larger current outputs in response to lower voltages. In addition to this, increased numbers of units were obtained in case of extracellular recordings from coated electrode at each of the stimulation voltage as shown in 4.2C.

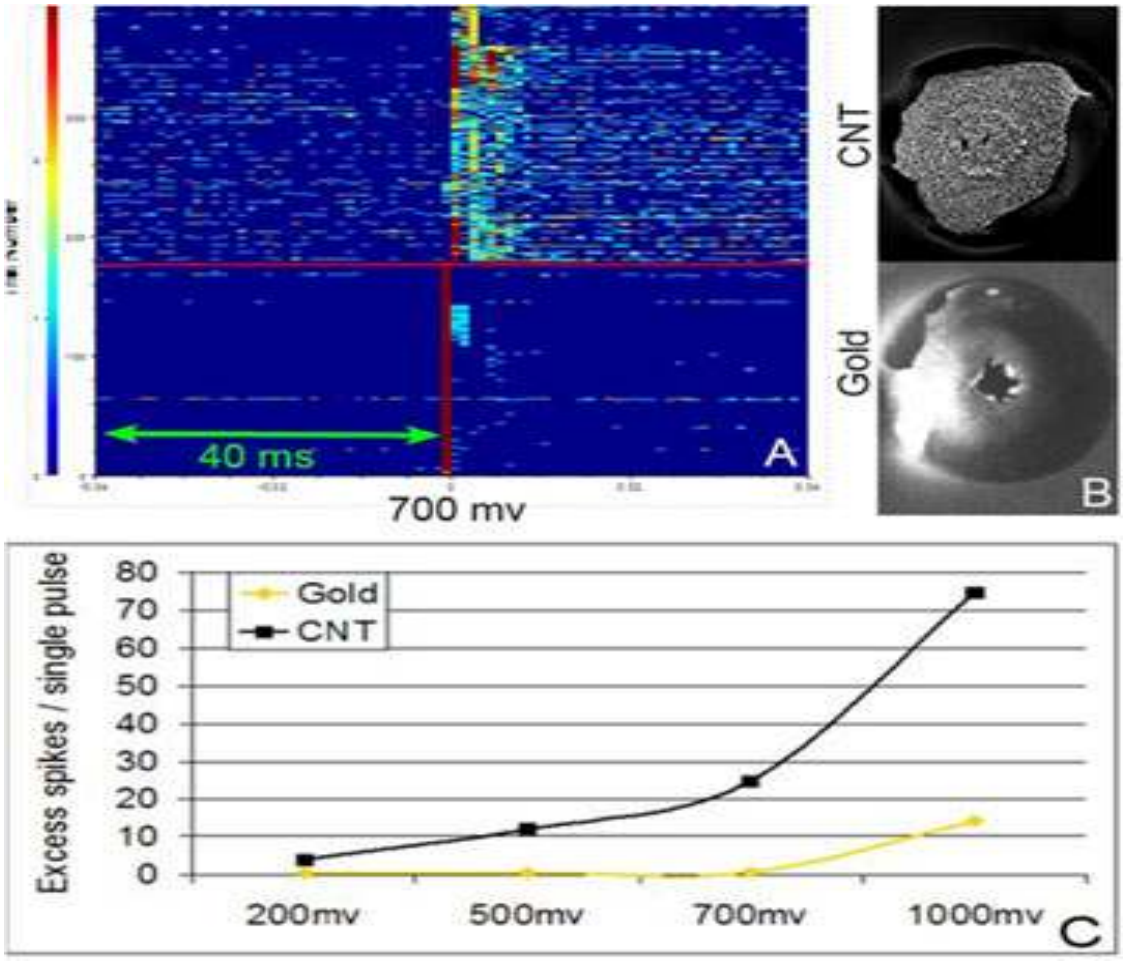

Figure 4.2 Enhancement in recording capabilities of metal electrodes after CNT coating: A is a peri-stimulus-time histogram constructed from over 400 stimuli introduced to the neuronal network through 24 separate electrodes (12 gold/12 CNT-coated)(B). C shows increased amount of signal recorded from coated electrodes represented by increased amount of spiking activity.

CNT coated electrodes exhibit increase in charge storage capacity as compare to metal electrodes since charge is stored in electrochemical double layer formed at the interface and not in the bulk material. Both of these mechanisms have limitation to amount of charge storage unlike conductive polymers which stores charge in form of ions, via a redox pseudocapacitive storage mechanism (Hughes, 2002). Thus we anticipate that future studies with incorporation of Carbon Nanotubes in conductive polymer would synergize the effect on capacitance while retaining the reduced impedance.

CHAPTER 5

CONCLUSION & FUTURE WORK

State of the art myoelectric prostheses lacked natural characteristics of the arm/hand like strength, flexibility and degree of freedom which minimized its usage by the amputees. This directed the development of sophisticated neuroprostheses that operates in a closed loop fashion in which voluntary actions guided by sensory feedback is neurally controlled. However these implants lack long term use due to its unstable interface which directly affects the effectiveness and functional efficiency of the prosthetic devices. Biggest challenge is to maintain stability of all the components of neuroprostheses with respect to time and function during implantation as well as during chronic usage (Koch 2007).

Histological and electrophysiological evidences support the fact that the regenerative multi-electrode array provides a stable neurointerface to the amputated peripheral nerves and opens the possibility of providing sensory feedback to the neural prostheses by selective stimulation of the regenerated nerve. Stable single/multi-unit activity from the regenerated axons of acute and chronically injured nerves demonstrates that the sciatic nerve regeneration was normal and uninterrupted. Lesser induction of inflammation and no insertion-related tissue trauma led to presence of regenerated axons closer to recording surface. In summary, our findings indicate that non-obstructive regenerative multielectrode arrays can guide nerve regeneration in close proximity to

their active sites eliciting minimal inflammation and providing early and relatively stable neurointerfacing to both acute and chronic injured peripheral nerves. Multi-electrode arrays used in regenerative paradigm have potential to be an effective peripheral interface for chronic implantations.

Several technical complications and challenges were faced in this study. Breaking of long interconnecting wires near the neck joint and thigh joints was the major hindrance to achieve long-term implantation of the electrodes in the rat sciatic nerve leading to short survival periods in some animals. The use of short length, flexible but robust interconnecting wires would mitigate these problems. A potential wireless system could be developed where one or more implantable devices would acquire signals from patient's neural pathways to provide direct control over the prosthetic arm in response to supplemental inputs from the same (Ghovanloo and Najafi 2007). In addition to this, since reorganization of regenerated axons differs from normal nerve physiology, we could not correlate electrophysiology data to what type of axons were firing. Further studies needs to be done to correlate behavioral aspects and neural activity by training the subject to perform one particular action in return of rewards and correspondingly study changes in pattern of neuronal firing in response to this action. Comprehensive study with different actions and stimulus is critical to anticipate desired action based on recording from the mixed nerve.

Studies were done in which regenerating axons were successfully enticed and guided to regrow in desired compartments by providing necessary neurotrophins. These studies tested sorting of only nociceptive and proprioceptive fibers which gives

information about pain sensation and spatial location of our limbs respectively. This experimental paradigm was further tested in vivo where the compartmentalized regenerative conduit with specific growth factors was used to segregate population of regenerating sensory and motor axons. It was anticipated that these segregated/enriched axons would then aid recording/stimulation of these neuronal sub-types with high specificity (Pettingill et al. 2007; Rejali et al. 2007; Yamagata et al. 2004). In future studies, specific signatures of motor and sensory neuronal firing can be obtained by recording from primary neuronal culture of DRG neurons and ventral motor neurons. Gelfoam based delivery system was not optimum since gradient was persistent only for 8 hours and spill over occurred after the same amount of time. Incorporation of controlled delivery system within the conduits using polymeric microsperes, nanoparticles or immobilization of growth factors by microcontact printing, microfluidic network (Hodgkinson et al. 2007) and patterning (Yu et al. 2008), would enhance the degree of sorting of axonal sub-types and would facilitate better interpretation of recorded signal from a mixed modality nerve.

Neural implants electrodeposited with carbon nanotubes showed improved electrochemical properties. Though drastic reduction in the electrode impedance was achieved in this study, influence of CNTs on charge storage capacity was not satisfactory. However coating of conductive polymers (CP) like polypyrrole and PEDOTs have shown dramatic increase in its charge storage capacity (Cui et al. 2003); however lacks the stability due to its weak mechanical properties and dissolubility in water (Reichert 2008). Thus polymer- CNT composite coatings can impart best electrochemical characteristics

and coating stability. Studies to develop supercapacitors have shown that CP-CNT composites facilitate maximum increase in the capacitance compared to only polymer or CNTs (Cosnier 2008; Wang 2005; Peng 2007). In addition to augmentation in signal conduction and stimulation ability, these coated electrodes could also be used for enzyme or biomolecules detection.

Studies have been done to optimize the electrode design to facilitate electrical recordings from peripheral nerves whose signals are small and decay rapidly with distance. Alternatively, new electrode designs such as tubular, semi-tubular, or spiral, which incorporate characteristics predicted by mathematical simulation studies designed to amplify the amplitude of the recorded nerve signals (Loeb 1977, Fitzgerald 2008) might prove to be helpful in obtaining a more sensitive neurointerface. Along with the interface, other components like biomimmetic arm, actuators, control circuit and processor needs to be dealt with.

REFERENCES

Anderson JM, Rodriguez A, and Chang DT. Foreign body reaction to biomaterials. *Semin Immunol* 20: 86-100, 2008.

Baichwal RR, Bigbee JW, and DeVries GH. Macrophage-mediated myelin-related mitogenic factor for cultured Schwann cells. *Proc Natl Acad Sci U S A* 85: 1701-1705, 1988.

Biran R, Martin DC, and Tresco PA. The brain tissue response to implanted silicon microelectrode arrays is increased when the device is tethered to the skull. *J Biomed Mater Res A* 82: 169-178, 2007.

Biran R, Martin DC, and Tresco PA. Neuronal cell loss accompanies the brain tissue response to chronically implanted silicon microelectrode arrays. *Exp Neurol* 195: 115-126, 2005.

Branner A, and Normann RA. A multielectrode array for intrafascicular recording and stimulation in sciatic nerve of cats. *Brain Res Bull* 51: 293-306, 2000.

Branner A, Stein RB, Fernandez E, Aoyagi Y, and Normann RA. Long-term stimulation and recording with a penetrating microelectrode array in cat sciatic nerve. *IEEE Trans Biomed Eng* 51: 146-157, 2004.

Branner A, Stein RB, and Normann RA. Selective stimulation of cat sciatic nerve using an array of varying-length microelectrodes. *J Neurophysiol* 85: 1585-1594, 2001.

Burnod Y, Grandguillaume P, Otto I, Ferraina S, Johnson PB, and Caminiti R. Visuomotor transformations underlying arm movements toward visual targets: a neural network model of cerebral cortical operations. *J Neurosci* 12: 1435-1453, 1992.

Campbell PK, Jones KE, Huber RJ, Horch KW, and Normann RA. A silicon-based, three-dimensional neural interface: manufacturing processes for an intracortical electrode array. *IEEE Trans Biomed Eng* 38: 758-768, 1991.

Ceballos D, Valero-Cabre A, Valderrama E, Schuttler M, Stieglitz T, and Navarro X. Morphologic and functional evaluation of peripheral nerve fibers regenerated through polyimide sieve electrodes over long-term implantation. *J Biomed Mater Res* 60: 517-528, 2002.

Chapin JK. Using multi-neuron population recordings for neural prosthetics. *Nat Neurosci* 7: 452-455, 2004.

Cohen S, Funkelstein L, Livet J, Rougon G, Henderson CE, Castellani V, and Mann F. A semaphorin code defines subpopulations of spinal motor neurons during mouse development. *Eur J Neurosci* 21: 1767-1776, 2005.

Cui X, Wiler J, Dzaman M, Altschuler RA, and Martin DC. In vivo studies of polypyrrole/peptide coated neural probes. *Biomaterials* 24: 777-787, 2003.

Dhillon GS, and Horch KW. Direct neural sensory feedback and control of a prosthetic arm. *IEEE Trans Neural Syst Rehabil Eng* 13: 468-472, 2005.

Dhillon GS, Kruger TB, Sandhu JS, and Horch KW. Effects of short-term training on sensory and motor function in severed nerves of long-term human amputees. *J Neurophysiol* 93: 2625-2633, 2005.

Dickson BJ. Molecular mechanisms of axon guidance. *Science* 298: 1959-1964, 2002.

Donoghue JP. Connecting cortex to machines: recent advances in brain interfaces. *Nat Neurosci* 5 Suppl: 1085-1088, 2002.

Donoghue JP, Nurmikko A, Black M, and Hochberg LR. *J Physiol* 579: 603-611, 2007.

Dubovy P. Schwann cells and endoneurial extracellular matrix molecules as potential cues for sorting of regenerated axons: a review. *Anat Sci Int* 79: 198-208, 2004.

Edell DJ. A peripheral nerve information transducer for amputees: long-term multichannel recordings from rabbit peripheral nerves. *IEEE Trans Biomed Eng* 33: 203-214, 1986.

Ernfors P, Lee KF, Kucera J, and Jaenisch R. Lack of neurotrophin-3 leads to deficiencies in the peripheral nervous system and loss of limb proprioceptive afferents. *Cell* 77: 503-512, 1994.

Evarts EV. Pyramidal tract activity associated with a conditioned hand movement in the monkey. *J Neurophysiol* 29: 1011-1027, 1966.

Fawcett JW, and Keynes RJ. Peripheral nerve regeneration. *Annu Rev Neurosci* 13: 43-60, 1990.

Fitzgerald, J.J., et al., Microchannels as axonal amplifiers. IEEE Trans Biomed Eng, 2008. 55(3): p. 1136-46.

Fu SY, and Gordon T. The cellular and molecular basis of peripheral nerve regeneration. *Mol Neurobiol* 14: 67-116, 1997.

Galvan-Garcia P, Keefer EW, Yang F, Zhang M, Fang S, Zakhidov AA, Baughman RH, and Romero MI. Robust cell migration and neuronal growth on pristine carbon nanotube sheets and yarns. *J Biomater Sci Polym Ed* 18: 1245-1261, 2007.

Ghovanloo M, and Najafi K. A wireless implantable multichannel microstimulating system-on-a-chip with modular architecture. *IEEE Trans Neural Syst Rehabil Eng* 15: 449-457, 2007.

Gonzalez C, and Rodriguez M. A flexible perforated microelectrode array probe for action potential recording in nerve and muscle tissues. *J Neurosci Methods* 72: 189-195, 1997.

Gordon T, Sulaiman O, and Boyd JG. Experimental strategies to promote functional recovery after peripheral nerve injuries. *J Peripher Nerv Syst* 8: 236-250, 2003.

Goshima Y, Ito T, Sasaki Y, and Nakamura F. Semaphorins as signals for cell repulsion and invasion. *J Clin Invest* 109: 993-998, 2002.

Griffith RW, and Humphrey DR. Long-term gliosis around chronically implanted platinum electrodes in the Rhesus macaque motor cortex. *Neurosci Lett* 406: 81-86, 2006.

Hochberg LR, Serruya MD, Friehs GM, Mukand JA, Saleh M, Caplan AH, Branner A, Chen D, Penn RD, and Donoghue JP. Neuronal ensemble control of prosthetic devices by a human with tetraplegia. *Nature* 442: 164-171, 2006.

Hodgkinson GN, Tresco PA, and Hlady V. The differential influence of colocalized and segregated dual protein signals on neurite outgrowth on surfaces. *Biomaterials* 28: 2590-2602, 2007.

Holecko MM, 2nd, Williams JC, and Massia SP. Visualization of the intact interface between neural tissue and implanted microelectrode arrays. *J Neural Eng* 2: 97-102, 2005.

House PA, MacDonald JD, Tresco PA, and Normann RA. Acute microelectrode array implantation into human neocortex: preliminary technique and histological considerations. *Neurosurg Focus* 20: E4, 2006.

Jelsma TN, and Aguayo AJ. Trophic factors. *Curr Opin Neurobiol* 4: 717-725, 1994.

Jerregard H, Nyberg T, and Hildebrand C. Sorting of regenerating rat sciatic nerve fibers with target-derived molecules. *Exp Neurol* 169: 298-306, 2001.

Kalaska JF, and Crammond DJ. Cerebral cortical mechanisms of reaching movements. *Science* 255: 1517-1523, 1992.

Karchewski LA, Kim FA, Johnston J, McKnight RM, and Verge VM. Anatomical evidence supporting the potential for modulation by multiple neurotrophins in the majority of adult lumbar sensory neurons. *J Comp Neurol* 413: 327-341, 1999.

Koch KP. Neural prostheses and biomedical microsystems in neurological rehabilitation. *Acta Neurochir Suppl* 97: 427-434, 2007.

Kovacs GT, Storment CW, and Rosen JM. Regeneration microelectrode array for peripheral nerve recording and stimulation. *IEEE Trans Biomed Eng* 39: 893-902, 1992.

Kuiken TA, Marasco PD, Lock BA, Harden RN, and Dewald JP. Redirection of cutaneous sensation from the hand to the chest skin of human amputees with targeted reinnervation. *Proc Natl Acad Sci U S A* 104: 20061-20066, 2007.

Lago N, Ceballos D, Rodriguez FJ, Stieglitz T, and Navarro X. Long term assessment of axonal regeneration through polyimide regenerative electrodes to interface the peripheral nerve. *Biomaterials* 26: 2021-2031, 2005.

Lago N, and Navarro X. Evaluation of the long-term regenerative potential in an experimental nerve amputee model. *J Peripher Nerv Syst* 12: 108-120, 2007.

Lago N, Udina E, Ramachandran A, and Navarro X. Neurobiological assessment of regenerative electrodes for bidirectional interfacing injured peripheral nerves. *IEEE Trans Biomed Eng* 54: 1129-1137, 2007a.

Lago N, Yoshida K, Koch KP, and Navarro X. Assessment of biocompatibility of chronically implanted polyimide and platinum intrafascicular electrodes. *IEEE Trans Biomed Eng* 54: 281-290, 2007b.

Lauer RT, Peckham PH, Kilgore KL, and Heetderks WJ. Applications of cortical signals to neuroprosthetic control: a critical review. *IEEE Trans Rehabil Eng* 8: 205-208, 2000.

Lebedev MA, and Nicolelis MA. Brain-machine interfaces: past, present and future. *Trends Neurosci* 29: 536-546, 2006.

Leung BK, Biran R, Underwood CJ, and Tresco PA. Characterization of microglial attachment and cytokine release on biomaterials of differing surface chemistry. *Biomaterials* 29: 3289-3297, 2008.

Lewicki MS. A review of methods for spike sorting: the detection and classification of neural action potentials. *Network* 9: R53-78, 1998.

Li LJ, Zhang J, Zhang F, Lineaweaver WC, Chen TY, and Chen ZW. Longitudinal intrafascicular electrodes in collection and analysis of sensory signals of the peripheral nerve in a feline model. *Microsurgery* 25: 561-565, 2005.

Loeb GE, and Peck RA. Cuff electrodes for chronic stimulation and recording of peripheral nerve activity. *J Neurosci Methods* 64: 95-103, 1996.

Loeb, G.E., W.B. Marks, and P.G. Beatty, Analysis and microelectronic design of tubular electrode arrays intended for chronic, multiple single-unit recording from captured nerve fibres. Med Biol Eng Comput, 1977. 15(2): p. 195-201.

Lovat V, Pantarotto D, Lagostena L, Cacciari B, Grandolfo M, Righi M, Spalluto G, Prato M, and Ballerini L. Carbon nanotube substrates boost neuronal electrical signaling. *Nano Lett* 5: 1107-1110, 2005.

Ludwig KA, Uram JD, Yang J, Martin DC, and Kipke DR. Chronic neural recordings using silicon microelectrode arrays electrochemically deposited with a poly(3,4-ethylenedioxythiophene) (PEDOT) film. *J Neural Eng* 3: 59-70, 2006.

Lundborg G, Dahlin LB, Danielsen N, and Nachemson AK. Tissue specificity in nerve regeneration. *Scand J Plast Reconstr Surg* 20: 279-283, 1986.

Lundborg G. Nerve Injury and Repair: Regeneration, Reconstruction and Cortical Reodelling. Elseivers 2004

McDonnall D, Clark GA, and Normann RA. Interleaved, multisite electrical stimulation of cat sciatic nerve produces fatigue-resistant, ripple-free motor responses. *IEEE Trans Neural Syst Rehabil Eng* 12: 208-215, 2004a.

McDonnall D, Clark GA, and Normann RA. Selective motor unit recruitment via intrafascicular multielectrode stimulation. *Can J Physiol Pharmacol* 82: 599-609, 2004b.

Mensinger AF, Anderson DJ, Buchko CJ, Johnson MA, Martin DC, Tresco PA, Silver RB, and Highstein SM. Chronic recording of regenerating VIIIth nerve axons with a sieve electrode. *J Neurophysiol* 83: 611-615, 2000.

Mensinger AF, and Highstein SM. Characteristics of regenerating horizontal semicircular canal afferent and efferent fibers in the toadfish, Opsanus tau. *J Comp Neurol* 410: 653-676, 1999.

Merrill DR, and Tresco PA. Impedance characterization of microarray recording electrodes in vitro. *IEEE Trans Biomed Eng* 52: 1960-1965, 2005.
Miller LA, Stubblefield KA, Lipschutz RD, Lock BA, and Kuiken TA. Improved myoelectric prosthesis control using targeted reinnervation surgery: a case series. *IEEE Trans Neural Syst Rehabil Eng* 16: 46-50, 2008.

Moqrich A, Earley TJ, Watson J, Andahazy M, Backus C, Martin-Zanca D, Wright DE, Reichardt LF, and Patapoutian A. Expressing TrkC from the TrkA locus causes a subset of dorsal root ganglia neurons to switch fate. *Nat Neurosci* 7: 812-818, 2004.

Mussa-Ivaldi FA, and Miller LE. Brain-machine interfaces: computational demands and clinical needs meet basic neuroscience. *Trends Neurosci* 26: 329-334, 2003.

Navarro X, Krueger TB, Lago N, Micera S, Stieglitz T, and Dario P. A critical review of interfaces with the peripheral nervous system for the control of neuroprostheses and hybrid bionic systems. *J Peripher Nerv Syst* 10: 229-258, 2005.

Navarro X, Rodriguez FJ, Labrador RO, Buti M, Ceballos D, Gomez N, Cuadras J, and Perego G. Peripheral nerve regeneration through bioresorbable and durable nerve guides. *J Peripher Nerv Syst* 1: 53-64, 1996.

Navarro X, Udina E, Ceballos D, and Gold BG. Effects of FK506 on nerve regeneration and reinnervation after graft or tube repair of long nerve gaps. *Muscle Nerve* 24: 905-915, 2001.

Negredo P, Castro J, Lago N, Navarro X, and Avendano C. Differential growth of axons from sensory and motor neurons through a regenerative electrode: a stereological, retrograde tracer, and functional study in the rat. *Neuroscience* 128: 605-615, 2004.

Nicolelis MA. Actions from thoughts. *Nature* 409: 403-407, 2001.

Nicolelis MA. Brain-machine interfaces to restore motor function and probe neural circuits. *Nat Rev Neurosci* 4: 417-422, 2003.

Nicolelis MA, Baccala LA, Lin RC, and Chapin JK. Sensorimotor encoding by synchronous neural ensemble activity at multiple levels of the somatosensory system. *Science* 268: 1353-1358, 1995.

Nicolelis MA, and Ribeiro S. Multielectrode recordings: the next steps. *Curr Opin Neurobiol* 12: 602-606, 2002.

Normann RA. Technology insight: future neuroprosthetic therapies for disorders of the nervous system. *Nat Clin Pract Neurol* 3: 444-452, 2007.

Patil PG, and Turner DA. The development of brain-machine interface neuroprosthetic devices. *Neurotherapeutics* 5: 137-146, 2008.
Pettingill LN, Richardson RT, Wise AK, O'Leary SJ, and Shepherd RK. Neurotrophic factors and neural prostheses: potential clinical applications based upon findings in the auditory system. *IEEE Trans Biomed Eng* 54: 1138-1148, 2007.

Polikov VS, Block ML, Fellous JM, Hong JS, and Reichert WM. In vitro model of glial scarring around neuroelectrodes chronically implanted in the CNS. *Biomaterials* 27: 5368-5376, 2006.

Polikov VS, Tresco PA, and Reichert WM. Response of brain tissue to chronically implanted neural electrodes. *J Neurosci Methods* 148: 1-18, 2005.

Raivich G, and Kreutzberg GW. Expression of growth factor receptors in injured nervous tissue. I. Axotomy leads to a shift in the cellular distribution of specific beta-nerve growth factor binding in the injured and regenerating PNS. *J Neurocytol* 16: 689-700, 1987.

Rejali D, Lee VA, Abrashkin KA, Humayun N, Swiderski DL, and Raphael Y. Cochlear implants and ex vivo BDNF gene therapy protect spiral ganglion neurons. *Hear Res* 228: 180-187, 2007.

Reichert W. Indwelling Neural Implants Strategies for contending with the in vivo environment. Frontiers in Neural Engineering, 2008.

Rich KM, Luszczynski JR, Osborne PA, and Johnson EM, Jr. Nerve growth factor protects adult sensory neurons from cell death and atrophy caused by nerve injury. *J Neurocytol* 16: 261-268, 1987.

Richardson RT, Thompson B, Moulton S, Newbold C, Lum MG, Cameron A, Wallace G, Kapsa R, Clark G, and O'Leary S. The effect of polypyrrole with incorporated neurotrophin-3 on the promotion of neurite outgrowth from auditory neurons. *Biomaterials* 28: 513-523, 2007.

Riso RR. Strategies for providing upper extremity amputees with tactile and hand position feedback--moving closer to the bionic arm. *Technol Health Care* 7: 401-409, 1999.

Roitbak T, and Sykova E. Diffusion barriers evoked in the rat cortex by reactive astrogliosis. *Glia* 28: 40-48, 1999.

Romero MI, Lin L, Lush ME, Lei L, Parada LF, and Zhu Y. Deletion of Nf1 in neurons induces increased axon collateral branching after dorsal root injury. *J Neurosci* 27: 2124-2134, 2007.

Romero MI, Rangappa N, Garry MG, and Smith GM. Functional regeneration of chronically injured sensory afferents into adult spinal cord after neurotrophin gene therapy. *J Neurosci* 21: 8408-8416, 2001.
Ruegg MA. Agrin, laminin beta 2 (s-laminin) and ARIA: their role in neuromuscular development. *Curr Opin Neurobiol* 6: 97-103, 1996.

Rutten WL. Selective electrical interfaces with the nervous system. *Annu Rev Biomed Eng* 4: 407-452, 2002.

Schmidt CE, and Leach JB. Neural tissue engineering: strategies for repair and regeneration. *Annu Rev Biomed Eng* 5: 293-347, 2003.

Schwartz AB. Cortical neural prosthetics. *Annu Rev Neurosci* 27: 487-507, 2004.

Seymour JP, and Kipke DR. Neural probe design for reduced tissue encapsulation in CNS. *Biomaterials* 28: 3594-3607, 2007.

Shimatani Y, Nikles SA, Najafi K, and Bradley RM. Long-term recordings from afferent taste fibers. *Physiol Behav* 80: 309-315, 2003.

Slot PJ, Selmar P, Rasmussen A, and Sinkjaer T. Effect of long-term implanted nerve cuff electrodes on the electrophysiological properties of human sensory nerves. *Artif Organs* 21: 207-209, 1997.

Smith GM, and Romero MI. Adenoviral-mediated gene transfer to enhance neuronal survival, growth, and regeneration. *J Neurosci Res* 55: 147-157, 1999.

Stoney SD, Jr., Thompson WD, and Asanuma H. Excitation of pyramidal tract cells by intracortical microstimulation: effective extent of stimulating current. *J Neurophysiol* 31: 659-669, 1968.

Sykova E, Vargova L, Prokopova S, and Simonova Z. Glial swelling and astrogliosis produce diffusion barriers in the rat spinal cord. *Glia* 25: 56-70, 1999.

Szarowski DH, Andersen MD, Retterer S, Spence AJ, Isaacson M, Craighead HG, Turner JN, and Shain W. Brain responses to micro-machined silicon devices. *Brain Res* 983: 23-35, 2003.

Thanos PK, Okajima S, and Terzis JK. Ultrastructure and cellular biology of nerve regeneration. *J Reconstr Microsurg* 14: 423-436, 1998.

Torebjork E. Nociceptor activation and pain. *Philos Trans R Soc Lond B Biol Sci* 308: 227-234, 1985.

Tykocinski M, Duan Y, Tabor B, Cowan RS. Chronic electrical stimulation of the auditory nerve using high surface area (HiQ) platinum electrodes. Hear Res. 2001 Sep;159(1-2):53-68.

Tyler DJ, and Durand DM. Chronic response of the rat sciatic nerve to the flat interface nerve electrode. *Ann Biomed Eng* 31: 633-642, 2003.

Tyler DJ, and Durand DM. Functionally selective peripheral nerve stimulation with a flat interface nerve electrode. *IEEE Trans Neural Syst Rehabil Eng* 10: 294-303, 2002.

Vallbo AB, Olsson KA, Westberg KG, and Clark FJ. Microstimulation of single tactile afferents from the human hand. Sensory attributes related to unit type and properties of receptive fields. *Brain* 107 (Pt 3): 727-749, 1984.

Varela-Echavarria A, Tucker A, Puschel AW, and Guthrie S. Motor axon subpopulations respond differentially to the chemorepellents netrin-1 and semaphorin D. *Neuron* 18: 193-207, 1997.

Vince V, Brelen ME, Delbeke J, and Colin IM. Anti-TNF-alpha reduces the inflammatory reaction associated with cuff electrode implantation around the sciatic nerve. *J Neuroimmunol* 165: 121-128, 2005.

Wang K, Fishman HA, Dai H, and Harris JS. Neural stimulation with a carbon nanotube microelectrode array. *Nano Lett* 6: 2043-2048, 2006.

Weis J, and Schroder JM. Differential effects of nerve, muscle, and fat tissue on regenerating nerve fibers in vivo. *Muscle Nerve* 12: 723-734, 1989.

Williams JC, Hippensteel JA, Dilgen J, Shain W, and Kipke DR. Complex impedance spectroscopy for monitoring tissue responses to inserted neural implants. *J Neural Eng* 4: 410-423, 2007.

Yamagata T, Miller JM, Ulfendahl M, Olivius NP, Altschuler RA, Pyykko I, and Bredberg G. Delayed neurotrophic treatment preserves nerve survival and electrophysiological responsiveness in neomycin-deafened guinea pigs. *J Neurosci Res* 78: 75-86, 2004.

Yu LM, Wosnick JH, and Shoichet MS. Miniaturized system of neurotrophin patterning for guided regeneration. *J Neurosci Methods* 171: 253-263, 2008.

Zhao Q, Drott J, Laurell T, Wallman L, Lindstrom K, Bjursten LM, Lundborg G, Montelius L, and Danielsen N. Rat sciatic nerve regeneration through a micromachined silicon chip. *Biomaterials* 18: 75-80, 1997.

BIOGRAPHICAL INFORMATION

The author, Kshitija Garde, completed her Bachelor of Engineering in Biomedical Engineering from one of the renowned colleges in Mumbai University, India. She then got enrolled in the Master of Science, joint program of Biomedical Engineering at University of Texas at Arlington/ University of Texas Southwestern Medical center in August 2006. In this period, she worked as the graduate research assistant in Plastic surgery department at UT Southwestern Medical School and volunteer in Texas Scottish Rite hospital, Dallas. She also gained practical industry experience while working on a cutting edge technology in Plexon Inc as a research intern. In the future she looks forward to pursue a career in the medical device field and eventually set up a company in the same area.